DEPARTMENT OF NAVAL ARCHITECTURE, OCEAN & MARINE ENGINEERING

University of Strathclyde Engineering

Theory and Numerical Modelling of Dynamic Ice-Structure Interaction for Ice-induced Vibrations

by

Xu Ji

A dissertation submitted in fulfilment
of the requirements for the degree of
Doctor of Philosophy

Glasgow, UK

2019

AUTHOR STATEMENT

This thesis is the result of the author's original research. It has been composed by the author and has not been previously submitted for examination which has led to the award of a degree.

Signed:

Date: /April/2019

For

Human Being

ACKNOWLEDGEMENTS

I would like to express my sincere gratitude to my supervisor, Dr. Erkan Oterkus, who guided me throughout my life during PhD journey and is always supportive of my decisions. I am very grateful to him for not only allowing me to carry out my research in full freedom, but also letting me become an independent person to life. I could not have what I have at this moment without all kinds of help and support from Dr. Erkan Oterkus.

I am also grateful to Dr. Dale G. Karr for the help, guidance and useful discussions at the University of Michigan, Ann Arbor, MI, USA during the final stage of my PhD research.

I would like to thank to the financial support provided by different institutions and organisations for supporting my PhD study. They are University Research Studentship and Postgraduate Research Travel Award from the University of Strathclyde; Mac Robertson Travel Scholarship from the University of Glasgow and the University of Strathclyde; Overseas PhD Students Grants from the Leche Trust; Registration Fee and Travel Support from 16th Techno-Ocean committee, Marine Technology Society and Institute of Electrical and Electronics Engineers Oceanic Engineering Society.

I am also grateful to the YouTube for providing the countless music that accompanied me days and nights as well as the inspirations of mind and appreciations of various beings behind them.

One's success requires the efforts of several generations. From a remote village in China to Glasgow in UK, I am sincerely grateful to my mother, Tong Wang, my father, Jingjun Ji and my grandparents for their strong beliefs on my success and their endless love.

Lastly, my grandpa, Guobin Ji. Hope you are proud of me.

ABSTRACT

This PhD work is done as a trilogy. In the first stage, a dynamic single degree-of-freedom ice-structure interaction model is developed based on a novel physical mechanism combination between self-excited vibration and forced vibration. Van der Pol equation, together with ice stress-strain rate curve and ice-velocity failure length are coupled to model the internal fluctuating nature of ice force in conjunction with the relative velocity caused by the structure as an external effect. Three basic modes of response were reproduced, such as intermittent crushing, frequency lock-in and continuous crushing. The results are in good match with experimental data at different ice velocities and different structural stiffnesses. Ice force frequency lock-in phenomenon during ice-induced vibrations (IIV) is also observed.

In the second stage, analysis on physical mechanism of ice-structure interaction is presented based on feedback mechanism and energy mechanism, respectively. Internal effect and external effect from ice and structure were both explained in the feedback branch. Based on reproduced results, energy exchanges at different configurations are computed from the energy conservation using the first law of thermodynamics. A conclusion on the predominant type of vibration when the ice velocity increases during the interaction process is forced, self-excited and forced in each three modes of responses. Ice force variations also shows that there is more impulse energy during the lock-in range. Moreover, IIV demonstrates an analogy of friction-induced self-excited vibration. The similarity between stress-strain curve and Stribeck curve shows that static and kinetic friction force variations are attributed to ice force characteristic, and can be used to explain the lower effective pressure magnitude during continuous crushing than the peak pressure during intermittent crushing.

In the third stage, a two-dimensional non-simultaneous ice failure model is developed. The concept of multiple ice failure zones is proposed to fulfil non-simultaneous crushing characteristics. The size of ice failure zone is assumed to become smaller with increasing ice velocity, which increases the occurrence of non-simultaneous ice failures. Similarly, the decreasing size of ice failure zone as velocity increases is explained as the reason of different ice failure modes shifting from large-area ductile bending to small-area brittle crushing. In addition, an analysis of the ice indentation

experiments indicates that the mean and minimum effective pressure have an approximately linear relationship with ice velocity, which testified the assumption on variations of ice failure zone in the model. The simulation results from a series of 134 demonstration cases show that the model is capable of predicting results at different ice velocities, structural widths and ice thicknesses.

To sum up, this Van der Pol based model is more powerful than the others in kind by far because of its accurate results, wide applicability and novel physical mechanism behind. Thus, the numerical models produced as part of this research can be helpful in ice failure analysis and in the design of ice-resistant structures.

CONTENTS

LIST OF FIGURES

LIST OF TABLES

NOMENCLATURE

$\dot{\varepsilon}$	Strain rate (s^{-1})
M	Mass (kg)
C	Damping coefficient (kg s^{-1})
K	Structural stiffness (kN m^{-1})
$\ddot{X}$	Structural acceleration (m s^{-2})
$\dot{X}$	Structural velocity (m s^{-1})
X	Structural displacement (m)
T	Time (s)
K_i	Effective ice stiffness (kN m^{-1})
δ, δ_h	Ice tooth deflection (m)
δ_{max}	Maximum ice tooth deflection (m)
F_{max}	Maximum ice force (kN)
$\ddot{Y}$	Ice acceleration (m s^{-2})
v, $\dot{Y}$	Ice velocity (m s^{-2})
Y	Ice displacement (m)
N	Number of failed ice tooth
p	Spacing between each ice tooth (m)
Z	Ice displacement increment of each extrusion (m)
p_f	Critical effective pressure (kPa)
D	Structural width (m)
H	Ice thickness (m)
F_e	Extrusion ice force (kN)
p_e	Extrusion pressure (kPa)
δ_h	Maximum ice tooth deflection (m)
X_0	Initial value of structural displacement (m)
F_c	Constant residual ice force (kN)
$\ddot{x}$	Normalized structural acceleration
$\dot{x}$	Normalized structural velocity
x	Normalized structural displacement
ξ	Damping ratio
ω_n	Angular natural frequency of structure (rad s^{-1})
σ	Ice stress (kPa)

A_0	Reference displacement (m)
q	Dimensionless fluctuation variable
ω_i	Angular frequency of ice force (rad s^{-1})
λ	Dimensionless coefficient
v_r	Relative velocity between ice and structure (m s^{-1})
v_t	Transition ice velocity in the middle of transition range (m s^{-1})
σ_{max}	Maximum stress at ductile-brittle range (kPa)
σ_d, σ_b	Minimum stress at ductile and brittle range (kPa)
α, β	Positive and negative indices to control the envelope profile
f_i	Ice failure frequency (Hz)
c_0	Ratio of v and L
L	Correlation or ice failure length (m)
f_v	Vortex-shedding frequency (Hz)
St	Strouhal number
v_f	Flow velocity (m s^{-1})
F	Ice force (kN)
A	Magnification factor
a, ε	Scalar parameters that control the q_i profile
B	Coefficient depending on ice properties
t	Normalized time
l	Normalized ice failure length
$\dot{y}$	Normalized ice velocity
ω_n	Angular natural frequency of structure (rad s^{-1})
f_n	Natural frequency of the structure (Hz)
τ	Reduced angular structural frequency
U_r	Reduced ice velocity
f_s	Frequency of structural displacement (Hz)
v_0	Reference velocity (m s^{-1})
d	Segment width (m)
n	Number of segments
K_0	Reference structural stiffness (kN m^{-1})
f_0	Reference frequency (Hz)
ω_i	Angular frequency of ice force (rad s^{-1})

f_i	Ice failure frequency (Hz)
Y	Ice displacement (m)
$\ddot{Y}$	Ice acceleration (m s^{-2})
$\dot{\varepsilon}$	Strain rate (s^{-1})
ΔW_t	Incremental work done by ice force
ΔE_m	Incremental change of mechanical energy in the structure
ΔE_d	Incremental heat dissipated by the structural damping
ΔE_p	Incremental change of potential energy in the structure
ΔE_k	Incremental change of kinetic energy in the structure
μ_s	Static friction coefficient
μ_k	Kinetic friction coefficient
L_i	Ice failure length of each ice strip (m)
c	Constant distributed normally with mean μ and variance σ_s^2
N_{strip}	Number of ice strips
W_i	Width of an ice failure zone (m)
q_i	Dimensionless fluctuation variable of each ice strip
ω_i	Angular frequency of ice force (rad s^{-1})
$\dot{Y}_i$	Velocity of each ice strip (m s^{-1})
Y_i	Displacement of each ice strip (m)
$\ddot{Y}_i$	Acceleration of each ice strip (m s^{-2})
μ_P	Mean effective pressure (kPa)
σ_P	Standard deviation of effective pressure (kPa)
F_μ	Mean value of ice force (kN)
F_σ	Standard deviation of ice force (kN)
$\Delta\mu_p,\ \Delta\sigma_p$	The difference between the results from model and experiment for μ_p and σ_p

CHAPTER

1. INTRODUCTION

The main aim of this chapter is to describe the background, motivation, and objectives of the research contained in this PhD thesis. This chapter is divided in four sections. In the first part, some basic information about ice research environment is given. In the second part (Section 1.2), the objectives of this research study are highlighted, while in the third part (Section 1.3), the structure of the thesis is presented. The required literature reviews are given in each corresponding chapter instead of giving them in the first chapter altogether.

1.1 Background and motivation

Ice-structure interaction drew people's attention since the oil exploration and exploitation in Cook Inlet, Alaska, 1962. Large variations of ice properties (Peyton, 1966) and large amplitude ice-induced vibrations (IIV) phenomenon (Blenkarn, 1970) were noticed and discussed from the data collected from this area. Offshore structures subjected to the action of drifting ice floes may experience several kinds of interactions with the ice. For instance, columns fixed to the seabed are commonly used as a form of ice-resistant offshore structures. Sometimes, this kind of structures experiences sustained interaction with the ice, which is called as ice-structure interaction, and severe vibration may occur under certain velocities (Yue and Guo, 2011). These vibrations, known as IIV, would lead to fatigue problems, along with safety issues and uncomfortable working and living conditions.

As arctic ice sheets are melting due to global warming, there is an increasing interest on the possibility of using a new route in the Arctic Ocean from Far East to Europe and oil and gas explorations in this area. Hence, it is essential to design ships and offshore structures which are resistant to possible ice impacts on the structure. However, because of the complex nature of ice and limited full-scale data, ice models and experiments show differences among each other (Sodhi, 1988) which makes the ice related research still a challenging area. Even after around half a century, the basic physical mechanism of the severest vibrations during ice-structure interaction, IIV, is still not fully understood.

1.2 Objectives of the research

The research described in the thesis has four main objectives:

- Creation of a novel single degree-of-freedom numerical model for dynamic ice-structure interactions based on a physical mechanism combination between self-excited vibration and forced vibration. The model is capable of capturing all different structural responses and the lock-in phenomenon in IIV. To the best of the author's knowledge, there are currently only two types of this kind of model. One is Matlock et al. (1971) based and further developed by Sodhi (1995) and Huang and Liu (2009). The other is Van der Pol based proposed by Wang and Xu (1991). However, there are some imperfection regarding the modelling that leads to inaccurate results and there is no further development of Van der Pol based model ever since. This goal is achieved in Ji and Oterkus (2016) as part of the research described in this thesis (Chapter 2).
- Development of the ice failure by correlating ice velocity and structural natural frequency into the model. The model is capable of accurately reproducing three basic modes of response, i.e. intermittent crushing, frequency lock-in and continuous crushing. This goal is achieved in Ji and Oterkus (2018) as part of the research described in this thesis (Chapter 3).
- Discussions and explanations of the physical mechanism of dynamic ice-structure interaction at three distinctive modes of response, especially the mechanics when IIV occurs. The scientific community has not reached a conclusion on the physical mechanism of IIV in the past half century. There are two theories, force vibration and self-excited vibration, and each supported by Dr. Devinder Sodhi of the U.S. Army Cold Regions Research and Engineering Laboratory and Prof. Mauri Määttänen of the Aalto University of Finland and the Norwegian University of Science and Technology. This is the first time that these two theories are brought together to explain the ice mechanics. This goal is achieved in Ji and Oterkus (2018) as part of the research described in this thesis (Chapter 3).
- Creation of a two-dimensional non-simultaneous dynamic ice-structure interaction model based on the model from Chapter 3 to produce better correlation with the experimental data. This goal is achieved in Ji et al. (2018)

as part of the research described in this thesis (Chapter 4).

In conclusion, the ultimate goal of this research is to produce unconventional and more effective numerical frameworks that can be helpful in ice-structure engineering in the shipping and offshore industry.

1.3 Structure of the thesis

This PhD work was done as a trilogy, as presented in the middle three chapters. This thesis is constituted by the following five chapters:

- Chapter 1. This chapter provides basic information about ice-structure interaction and its impact on marine structures, which justify the need for further research in this field. In this manner, the benefits of numerical simulations are highlighted and the objectives of research and the organization of this thesis are described.
- Chapter 2. This chapter describes a novel Van der Pol based single degree-of-freedom model along with the results and discussions. Moreover, a literature review of current single degree-of-freedom numerical models used and basic mechanical features of ice failure are given at the beginning of this chapter. This chapter is an amended version of Ji and Oterkus (2016).
- Chapter 3. This chapter describes a further developed model based on the previous one by correlating ice velocity and structural natural frequency into the model. Moreover, the physical mechanism of dynamic ice-structure interaction at three distinctive modes of response is discussed and explained, especially the mechanics when IIV occurs. This chapter is an amended version of Ji and Oterkus (2018).
- Chapter 4. This chapter describes a further developed model based on the previous one by extending the one-dimensional into two-dimensional non-simultaneous model. Moreover, a literature review of non-simultaneous ice failure is introduced at the beginning of this chapter. This chapter is an amended version of Ji et al. (2018).
- Chapter 5. This chapter reviews the research objectives, summarizes the major findings, highlights the novelty and contribution of this research study of the field, discusses the gaps and the recommended future work, and closes with final remarks.

CHAPTER

2. A DYNAMIC ICE-STRUCTURE INTERACTION MODEL FOR ICE-INDUCED VIBRATIONS BY USING VAN DER POL EQUATION

In this chapter, a single degree-of-freedom ice-structure interaction model, ice force oscillator model, is developed based on a novel physical mechanism combination between self-excited vibration and forced vibration. Van der Pol equation, together with ice stress-strain rate curve and ice-velocity failure length are utilized to model the internal fluctuating nature of ice force in conjunction with the relative velocity and relative displacement caused by the structure as an external effect.

Reasons of IIV proposed by researchers can be divided into two categories; negative damping (Blenkarn, 1970; Määttänen, 1981) and resonance (Sodhi, 1988). Ice force frequency lock-in, when ice force frequency is strongly dominated by structural natural frequency, exists in both of these explanations (Huang and Liu, 2009; Määttänen, 1983; Wang and Xu, 1991; Yue and Guo, 2011). Both these two types of IIV are considered as self-excited vibration by the majority as opposed to forced vibration. It has been very debatable that whether resonance is either self-excited vibration or forced vibration for almost 50 years, claimed by Määttänen and Sodhi, respectively. Määttänen (2015) further mentioned that if the structure is not flexible enough, there should not be any self-excited vibration for the resonance caused by frequency lock-in. On the other hand, Sodhi (1988) discussed this as forced vibration because ice force still exists even when the structure is stopped from moving, see also Timoshenko and Young (1937) and definitions from Den Hartog (1947):

- In self-excited vibration, the alternating force that sustains the motion is created or controlled by the motion itself. When the motion stops, the alternating force disappears.
- In forced vibration, the sustaining alternating force exists independently apart from the motion and persists even when the vibratory motion is stopped.

From ice point of view, in forced vibration model, ice has its own failure characteristic and is not associated with either structural properties or structural motion variables.

On the other hand, in self-excited vibration, ice force is controlled by not only ice itself, but also structural motions. Since it is a fact that ice has its own characteristics, structural properties or motion variables will definitely be involved when ice is in contact with a structure and ice failure occurs. So, regardless of the structure being rigid or flexible, wide or narrow, vertical or conical, the main issue is how strong these structural effects can be added to the original ice failure behaviour. This is the reason why forced vibration or self-excited vibration mechanisms are predominant from time to time.

2.1 Numerical models in the literature

Numerical modelling of ice-structure interaction is a difficult process because of various ice properties, lack of data and unclear ice failure mechanism. Some effective single degree-of-freedom ice-structure interaction models have been developed since 1960s, in which structure is usually modelled as a mass- spring-damper system and different models have different forcing terms on the right-hand side of equation of motion.

2.1.1 Matlock et al. (1971)

Matlock et al. (1971) proposed the first ice-structure interaction numerical model along with a revolutionary idea that ice breaks into a certain size. As shown in Figure 2.1, ice is modelled as a series of brittle-elastic tooth equally spaced laying on a conveyor belt that moves towards the structure at a constant speed. Each of these elements interacts with the mass and exerts a force on the structure that is proportional to the tooth deflection. The force is assumed to increase linearly up to a maximum value, where ice tooth is assumed to fracture instantaneously at the maximum deflection and release the load on the structure. Then, the following tooth will continue after the first break and the process continues.

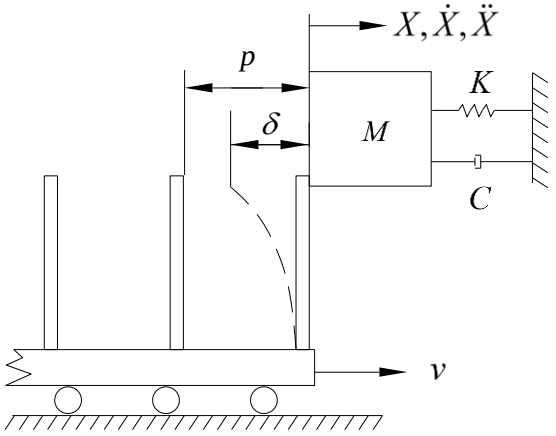

Figure 2.1. Schematic sketch of Matlock et al. model.

The equivalent equation of motion for this model is

$$M\ddot{X} + C\dot{X} + KX = K_i\delta \tag{2.1}$$

where M is the mass of the structure, X is the displacement of the structure, the "dot" symbol represents the derivative with respect to time T, C is the structural damping coefficient, K is the structural stiffness, $K_i = \delta_{max}/F_{max}$ can be considered as an effective stiffness of an ice sheet, $\delta = Y - X - (N-1)p$ is the ice tooth deflection, δ_{max} is the maximum ice tooth deflection, F_{max} is the maximum ice force, $Y = vT$ is the displacement of ice, v is the ice velocity, N is the number of failed ice tooth and p is the spacing between two ice teeth.

Structural displacement at low and high ice velocities of 0.127 m s^{-1} and 1.27 m s^{-1} are reproduced and has the same match of amplitude and frequency with those in Matlock et al. (1971), as shown in Figures 2.2 (a) and (c), in which the corresponding ice force time history are also plotted. As shown in Figure 2.3, spectral analysis of Figure 2.2 is done to show the frequency variation of ice force and structural displacement. Structural natural frequency of 3 *Hz* is plotted in red to tell resonant condition. The model is capable of capturing steady-state structural response at intermediate ice velocities of 0.7 m s^{-1}, as shown in Figure 2.2 (b). Spectral response of both ice fore and structural response shown that they are locking at around the structural natural frequency, as shown in Figure 2.3 (b), indicating a resonance condition occur.

However, as shown in the time history plotting, the force is not like as the real ice force. Though there is saw-tooth pattern, it represents each ice tooth failure in micro scale rather than macro failure, which leads to a much higher ice force frequency than the structural displacement frequency, as shown in Figure 2.3.

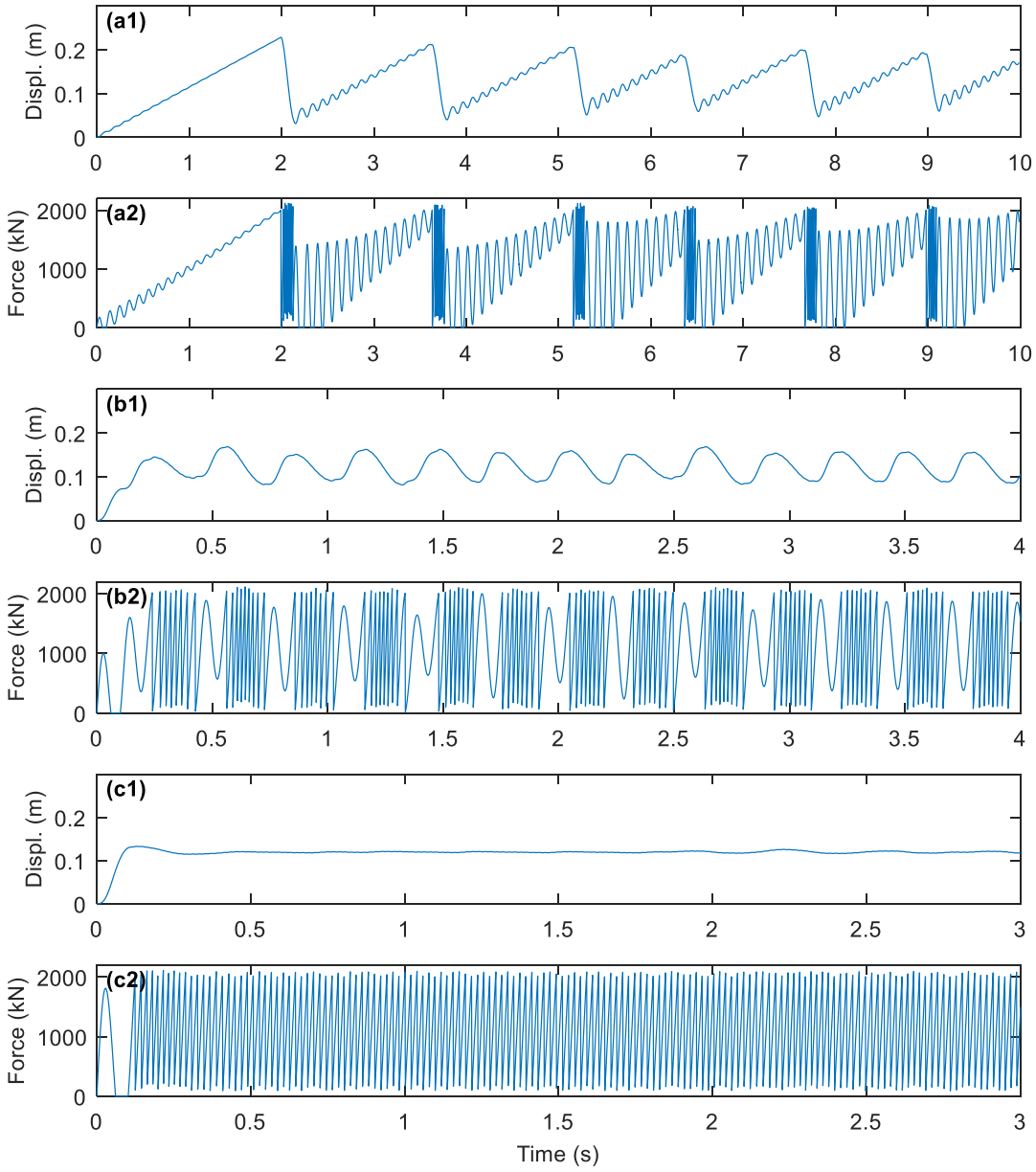

Figure 2.2. Time vs. structural displacement. (a) v=0.0127 m s^{-1}, (b) v=0.7 m s^{-1} and (c) v=1.27 m s^{-1}.

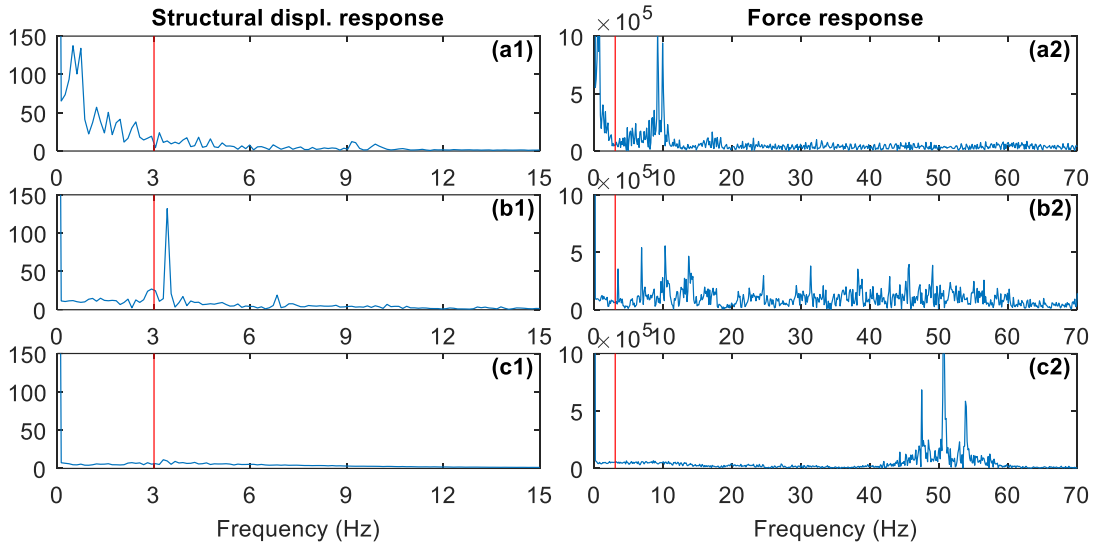

Figure 2.3. Structural displacement and force spectrum. (a) v=0.0127 m s^{-1}, (b) v=0.7 m s^{-1} and (c) v=1.27 m s^{-1}.

2.1.2 Sodhi (1995)

Coburn et al. (1984) found ice force dropped back to around one third of the maximum value instead of zero after the failure and modified the Matlock forcing term as $[(2/3)K_i\delta + 1/3F_{max}]$. Sodhi (1995) proposed an alternative approach for three different phases during each ice crushing cycle. These are a loading phase, an extrusion phase and a separation phase and three different equations are used accordingly in Eq. (2.2). He also explained that Matlock et al. (1971) considered only loading and separation phase in their model.

$$M\ddot{X} + C\dot{X} + KX = \begin{cases} K_i\delta \le p_f DH \\ F_e, \quad \dot{X} \le \dot{Y} \\ 0, \quad \delta \le 0 \end{cases} \tag{2.2}$$

K_i is the effective stiffness of the ice sheet, $\delta = Y - X - Z$ is the penetration of ice, which can be considered as the deflection in Matlock model, Y is the displacement of ice, Z is the displacement increment of ice at the end of an extrusion, p_f is the critical effective pressure at which the ice fails and is incapable of supporting the imposed loads at that instant, $F_e = p_e DH$ is the extrusion force, p_e is the extrusion pressure, D is the structural width, and H is the ice thickness.

2.1.3 Huang and Liu (2009)

The model proposed by Huang and Liu (2009) shared similar three phases with Sodhi's and added the force in extrusion phase in the loading phase as well.

$$M\ddot{X} + C\dot{X} + KX = \begin{cases} K_i\delta_h + F_c, & 0 \le \delta < \delta_{\max} \text{ and } \dot{X} \le \dot{Y} \\ F_c, & \delta_{\max} \le \delta < p \text{ and } \dot{X} \le \dot{Y} \\ 0, & \dot{X} > \dot{Y} \end{cases} \tag{2.3}$$

where $\delta_h = X_0 + \delta$, X_0 the initial value of structural displacement, F_c is a constant residual force. By using this model, ice force frequency lock-in phenomenon can be captured during IIV. The structural response also varies mainly depend on initial conditions such as initial structural velocity and initial structural displacement and can be very much different by changing the initial conditions.

2.1.4 Wang and Xu (1991)

Wang and Xu (1991) first utilized the Van der Pol equation as an ice force oscillator to simulate periodic and self-excited natures, which is the periodic force-time function that is missing in Mattock model. The coupled equation of motion and ice force oscillator are expressed in a dimensionless form as

$$\begin{cases} \ddot{x} + 2\xi\omega_n\dot{x} + \omega_n^2 x = (DH\sigma / A_0 M)q \\ \ddot{q} + \omega_i(-\alpha_0 - \gamma_0 q + \beta_0 q^2)\dot{q} + \omega_i^2 q = (\omega_i^2 q_0 / V_0)(v - \dot{x}) \end{cases} \tag{2.4}$$

where $x = X/A_0$, A_0 is a reference displacement, ξ is the damping ratio, D is the structural diameter, H is the ice thickness, σ is the ice stress, ω_i is the angular frequency of ice force and α_0, β_0, γ_0, ω_0, q_0 are determined from a model test in advance.

Wang and Xu (1991) claimed that frequency lock-in can be captured by using this model. However, as shown in Figure 2.4, the reproduced results of structural displacement frequency show a jump to the structural natural frequency then increases with the velocity instead of locking at the structural natural frequency.

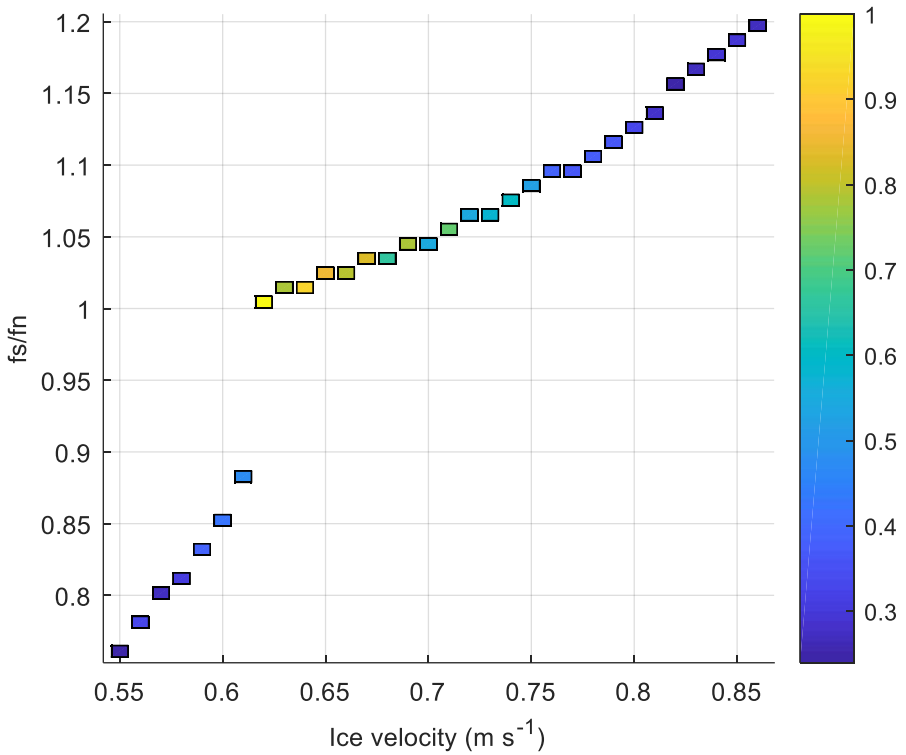

Figure 2.4. Ice velocity vs. ratio between structural displacement frequency $\boldsymbol{f_s}$ and $\boldsymbol{f_n}$.

2.2 Mechanical features of ice crushing

Different ice failure properties can cause different distinctive forces either on frequency or amplitude under different velocities (Blenkarn, 1970; Kärnä, 2007; Sodhi and Haehnel, 2003; Timco and Johnston, 2004) .

2.2.1 Ice stress-strain rate curve

It is found and proved that ice uniaxial stress or indentation stress is a function of the strain rate, as shown in Figure 2.5 (Blenkarn, 1970; Michel and Toussaint, 1978; Palmer et al., 1983; Sodhi and Haehnel, 2003). The strain rate is defined by $v_r/\lambda D$, where the dimensionless coefficient λ varies from 1 to 4 and D is the structural width (Yue and Guo, 2011). It can be expressed by two separate dimensional power functions:

$$\sigma = \begin{cases} (\sigma_{\max} - \sigma_d)(v_r / v_t)^{\alpha} + \sigma_d, & v_r / v_t \le 1 \\ (\sigma_{\max} - \sigma_b)(v_r / v_t)^{\beta} + \sigma_b, & v_r / v_t > 1 \end{cases} \tag{2.5}$$

where σ_{max} is the maximum stress at ductile-brittle range, σ_d and σ_b are the minimum stress at ductile range and maximum stress at brittle range, respectively, α and β are

positive and negative indices to control the envelope profile, respectively, and v_t is the transition ice velocity approximately in the middle of the transition range.

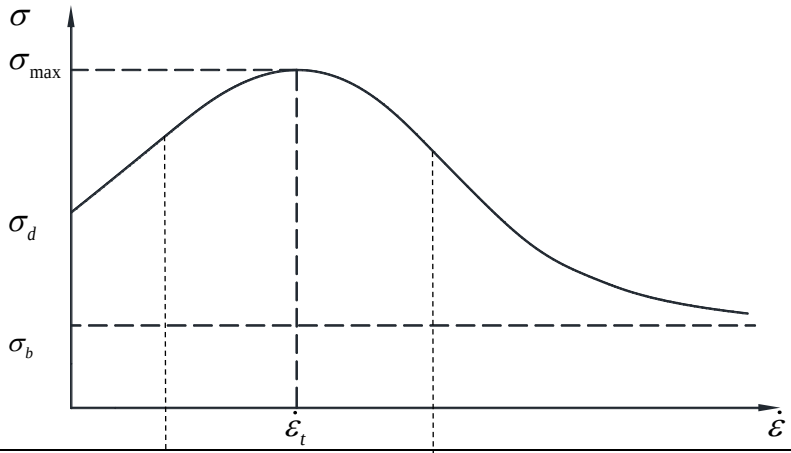

Ice	Ductile	Ductile-brittle	Brittle
	Intermittent crushing	Frequency lock-in	Continuous crushing
Structure	Quasi-static	Steady-state	Random

Figure 2.5. Strain rate vs. uniaxial or indentation stress corresponding to ice failure and structural response mode.

2.2.2 Ice failure length

Observations show that ice fails in wedge shape after one loading phase with a characteristic frequency at both full-scale and small-scale experiments. During the loading phase, micro-cracks inside the ice accumulate. When the density of micro-cracks reaches a critical level, ice is incapable of taking more load, leading to a coalescence of ice cracks in a whole amount, which is called unloading phase (Yue and Guo, 2011). Kärnä et al. (1993) used high speed camera and observed that ice fails at a certain amount after each loading phase. Neill (1976) reviewed numerous data and emphasized that ice fails by following a certain size distribution and ice velocity controls the ice failure frequency. Sodhi and Morris (1986) conducted small-scale tests pushing different diameter rigid cylinders at different velocities against ice sheets with different thicknesses, and found that the ice failure frequency is strongly proportional to ice velocity and slightly inversely proportional to structural diameter, and proposed that

$$f_i = c_0 \frac{v}{H} \tag{2.6}$$

where f_i is the ice failure frequency, H is the ice thickness. c_0 is the ratio of the ice thickness to ice failure length L, i.e. $c_0 = H/L$, and it ranges from 2 to 5, with an average value of around 3. Tong et al. (2001) conducted another similar series of small-scale tests and found the same trend. Palmer et al. (2010) reviewed both full-scale and small-scale data and proposed that the dimensionless velocity-thickness ratio parameter is more consistent than velocity-diameter ratio parameter to define different structural response modes.

2.2.3 Similarity with vortex-induced vibrations

As a result of the ice failure mechanism described in the previous section, ice-induced vibrations is often discussed as analogous to vortex-induced vibrations (Johansson, 1981; Palmer et al., 2010). The fluctuating nature of vortex shedding is similar to that of ice failure, causing periodic force upon structure. Furthermore, the similarity between vortex-shedding spacing and ice failure length leads to the analogical frequency calculation to Eq. (2.6) (Sodhi, 1988), in which vortex-shedding frequency f_v can be defined as $f_v = St \cdot v_f/D$, where St is the Strouhal number describing the oscillating flow mechanism and v_f is the flow velocity.

2.3 Model description

As shown in Figure 2.6, the structure is modelled as a mass-spring-damper system. Ice is moving towards the structure at a constant velocity. Ice force is calculated by area times stress. Ice failure is controlled by a periodic force-time oscillator, Van der Pol equation, which is used to model the saw-tooth shape of ice force fluctuation profile to demonstrate its internal natural failure behaviour, coupling the relative velocity v_r to correlate the strain energy into ice during both loading and unloading phases (Wang and Xu, 1991). Apart from utilization of the ice stress-strain rate relationship given in Eq. (2.5), another main advantage of the current approach is that the relative displacement between ice and structure is also considered during computations because compressive stress will transfer to ice deformation. When the deformation exceeds the natural ice failure length, ice will also fail, overcoming the overlook of external structural effect on ice failure in Wang and Xu's model. So, in addition to the Van der Pol oscillator, ice will also fail instantaneously when the relative displacement is larger than ice failure length, L. Therefore, ice will fail under both internal and external effects.

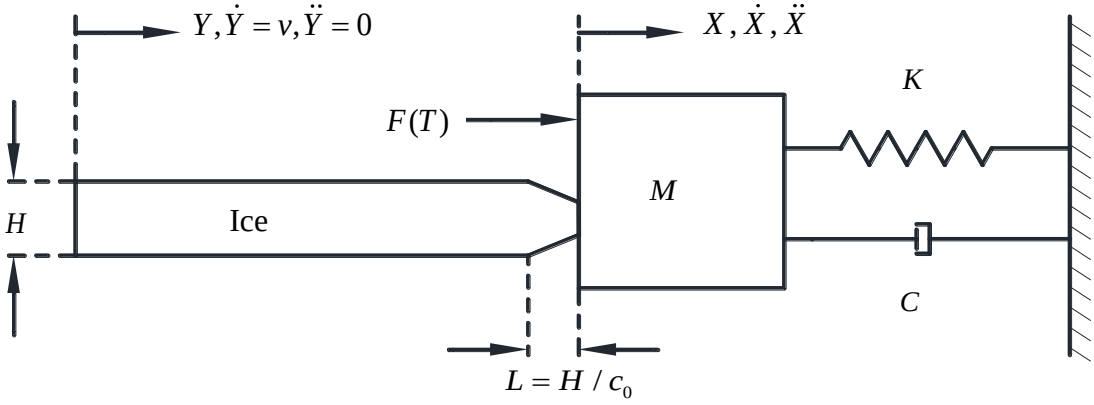

Figure 2.6. Schematic sketch of dynamic ice-structure model.

Therefore, this single degree-of-freedom ice-structure interaction model can be represented by using three equations. These are equation of motion and Van der Pol equation, i.e.

$$\begin{cases} M\ddot{X} + C\dot{X} + KX = F(T) = ADH\sigma(q + a) \\ \ddot{q} + \varepsilon\omega_i(q^2 - 1)\dot{q} + \omega_i^2 q = \dfrac{B\omega_i}{H}(\dot{Y} - \dot{X}) \end{cases} \tag{2.7}$$

in conjunction with the ice stress-strain rate relationship given in Eq. (2.5). In Eq. (2.7), X is the displacement of the structure, the "dot" symbol represents the derivative with respect to time T, A is the magnification factor adjusted from experimental data, D is the structural width, q is the dimensionless fluctuation variable, a and ε are scalar parameters that control the lower bound of ice force value and saw-tooth ice force profile, respectively, $\omega_i = 2\pi f_i$ is the angular frequency of ice force, B is a coefficient depending on ice properties and Y is the displacement of ice. Introducing the normalized quantities: $t = T\omega_i$, $x = X/H$, $l = L/H$, $\dot{y} = \dot{Y}/(\omega_i H)$, Eq. (2.7) can be transformed into dimensionless form as

$$\begin{cases} \ddot{x} + 2\xi\tau\dot{x} + \tau^2 x = \dfrac{AD\sigma\tau^2}{K}(q + a) \\ \ddot{q} + \varepsilon(q^2 - 1)\dot{q} + q = B(\dot{y} - \dot{x}) \end{cases} \tag{2.8}$$

where $\xi = C/(2M\omega_n)$ is the damping ratio, $\omega_n = \sqrt{K/M}$ is the angular natural frequency of the structure, $\tau = \omega_n/\omega_i$ is the reduced angular structural frequency which lead to the reduced ice velocity U_r as

$$\tau = \frac{\omega_n}{2\pi c(v_i / H)} = \frac{1}{cU_r},\ U_r = \frac{2\pi}{\omega_n}\frac{v}{H} = \frac{v}{f_n H} \tag{2.9}$$

When ω_i is close to ω_n, synchronization will occur defining a lock-in situation. Moreover, when $\tau = 1$ at $U_r = 1/c$, a perfect lock-in will occur.

2.4 Results

To date, studies have mainly focused on the ice velocity effect on ice force and structural dynamic behaviour. Coupled system configuration parameters are determined from the tests described in Huang et al. (2007) and specified as:

$D = 0.076$ m, $\omega_n = 39.27$ rad s^{-1}, $K = 27.44$ kN m^{-1}, $H_1 = 0.048$ m, $H_2 = 0.024$ m,
$\xi = 0.15$, A $= 0.068$, $a = 2$, $\varepsilon = 3.17$, $B = 0.1$, $c_0 = 3$,
$\sigma_{\max} = 110$ kPa, $\sigma_d = 84$ kPa, $\sigma_b = 65$ kPa, $\alpha = 0.2$, $\beta = -1.5$, $v_t = 0.15$ m s^{-1}.

During the steady-state vibration, the maximum structural velocity is found to have approximately a linear relationship with the ice velocity in many experiments (Kärnä, 2001). Figure 2.7 shows a good match for both the amplitude and the different structural response mode under different ice velocities. Steady-state vibration range in Huang et al. (2007) test (black line) is from 0.11 m s^{-1} to 0.205 m s^{-1} and from 0.08 m s^{-1} to 0.22 m s^{-1} in the present model (red line), which is determined from the corresponding ice force frequency lock-in range in Figure 2.9 (red line). On the left and right side of this range are quasi-static mode and random response mode, respectively.

Following this linear relationship, Kärnä and Trunen (1990) found that there are different upper limit and velocity range for different ice thicknesses according to the field records. Therefore, as another configuration, ice thickness is considered to be $H_2 = 0.024$ m, which is the half of the original thickness. Results for this case (blue line) are shown in Figure 2.7. In this case, maximum structural velocity reduces by half because half thickness reduces compressed area by half leading to half loading force. In addition, ice failure length also decreases by half leading to ice failure frequency twice higher and makes the resonance or ice force frequency lock-in range twice earlier, which is from 0.04 m s^{-1} to 0.11 m s^{-1} as opposed to from 0.08 m s^{-1} to 0.22 m s^{-1} for $H_1 = 0.048$ m. The variations in amplitude and range agree well with Kärnä and Trunen's observations, i.e. scaling down the behaviour observed in the original case to approximately one half.

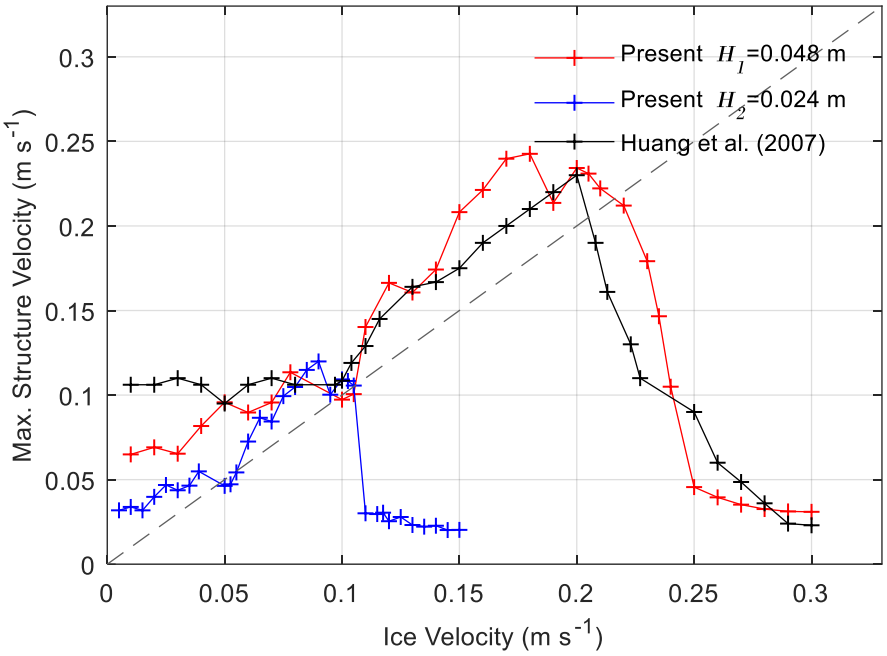

Figure 2.7. Ice velocity vs. the maximum structural velocity.

To show the ice force (red line) and structural response (blue line) transition during time histories, three representative velocities are picked from three distinctive structural response mode regions, as shown in Figure 2.8. Both of them captured the key characteristic behaviours observed in experimental tests done by Huang et al. (2007). Moreover, overall behaviour, i.e. saw tooth profile, sinusoidal structural response, and how the ice force and structural response change with ice velocity, are in good agreement both qualitatively and in most cases quantitatively with experimental results for a model ice and what many researchers cited in this paper including Matlock et al. (1971) and Kärnä (2001). In quasi-static region, shown in Figure 2.8(a), ice sheet fails in bending with ductile behaviour where a slow loading to the maximum is then followed by a quick unloading. At this stage, ice force and structural displacement are in phase with each other.

When ice speed increases to a critical value corresponding to the transitional ice velocity at the lower limit of the ice force frequency lock-in range as shown in Figure 2.8 (b), where ice fails between bending and crushing with ductile-brittle behaviour, loading and unloading takes less time. In addition to the ice internal natural failure behaviour defined in Eq. (2.6), failure as a result of the real-time ice-structure external effect is more significant, in which sudden unloading takes place sometimes due to the

fact that relative displacement exceeds the tolerable ice failure length. Consequently, ice force frequency will stay in this range leading to a resonance condition for a fairly large range as Yue and Guo (2011) observed in the field, where ice force and structural displacement are 90 degrees out-of-phase. In other words, ice and structure are moving in the same direction and structure is accelerated by the ice during loading phase. During the unloading phase, ice and structure are moving in the opposite direction. Moreover, the structure is decelerated by the ice as well since ice deformation will cause failure to occur when the compressive stress exceeds a condition that the natural failure length can tolerate. Figure 2.8 (c) is another vibration where this failure leading to the uniform peak value. These two types of structural vibrations can also be found in Huang and Liu (2009).

When ice speed exceeds another critical value corresponding to the transitional ice velocity at the upper limit of the ice force frequency lock-in range, ice will fail as crushing with brittle behavior. Then structure responds at small amplitude with relatively small predominant frequency compared with those at lower velocities, as shown in Figure 2.8 (d) and Figure 2.10, respectively.

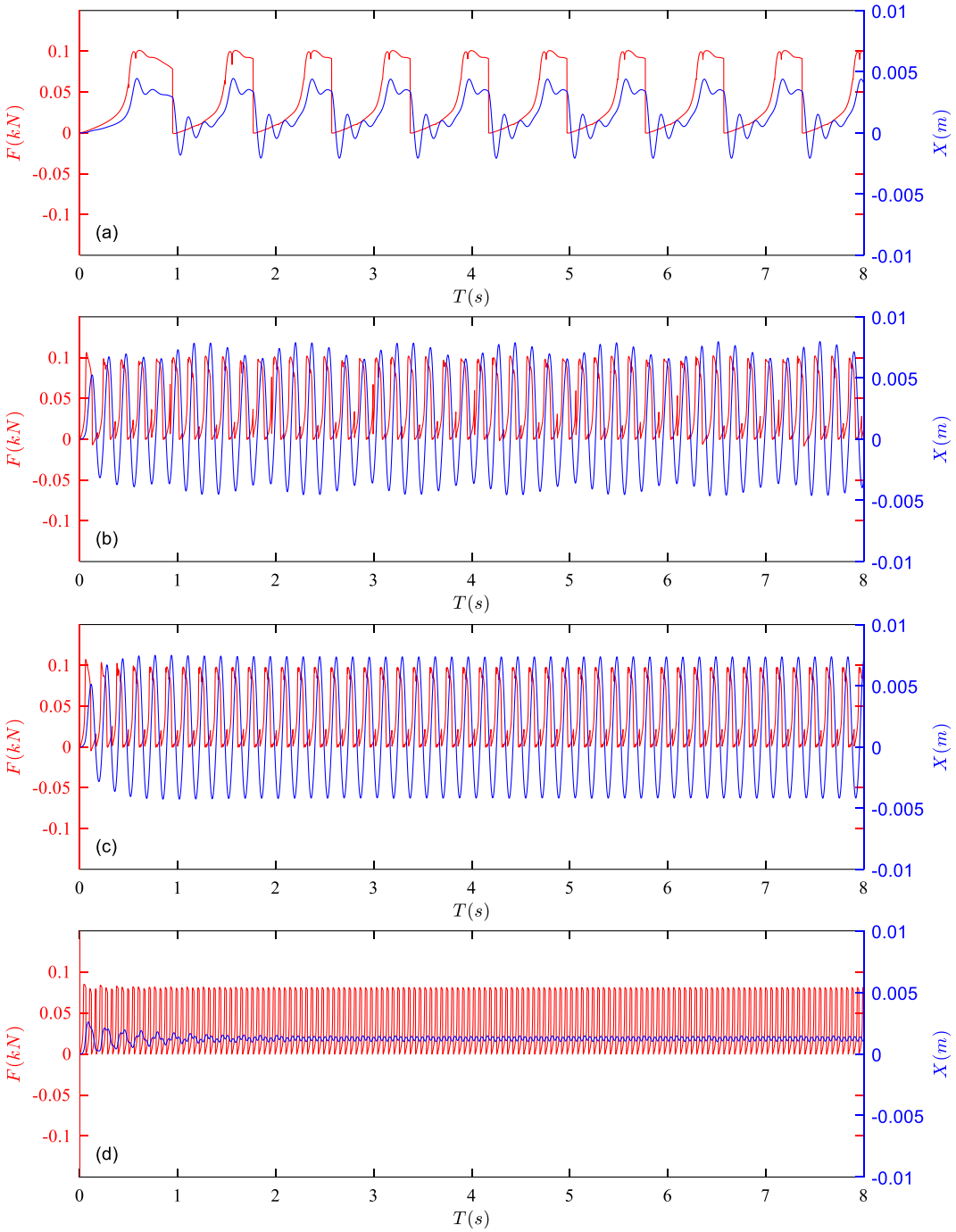

Figure 2.8. Time vs. ice force (red line) and structural displacement (blue line). (a) Quasi-static at v = 0.02 m s^{-1}, (b) Steady-state at v = 0.17 m s^{-1}, (c) Steady-state at v = 0.19 m s^{-1}, and (d) Random at v = 0.29 m s^{-1}.

2.5 IIV phenomenon

Ice force frequency lock-in is a significant phenomenon during IIV process. By transforming the time-history forces to spectrum analysis using fast Fourier transform

method, the predominant ice force frequencies under two different ice thicknesses are shown in Figure 2.9. Two lines at different thicknesses are following almost exactly the same pattern after the ice velocity is normalised to reduced velocity, especially for the frequency locking in range, from U_r =0.267 (0.06 m s^{-1}) to 0.733 (0.24 m s^{-1}) when H_1 =0.048 m and from U_r =0.3 (0.07 m s^{-1}) to 0.7 (0.23 m s^{-1}) when H_2 =0.024 m. This range matches well with the range suggested by Palmer et al. (2010) varying from 0.01 to 0.4 and to 0.8 occasionally. Moreover, most of the lock-in frequencies are slightly lower than the structural natural frequency that can also be confirmed from Kärnä et al. (2013). On the left and right side of this region are quasi-static and random modes, in which the ice force frequency in these two ranges is following a linear relationship with the ice velocity, and the slope is equal to c, as defined in Eq. (2.6). This similar lock-in range prediction can also be found in Huang and Liu (2009), whereas there is no need to define the initial conditions specifically in the present model and system will adjust to stable conditions automatically.

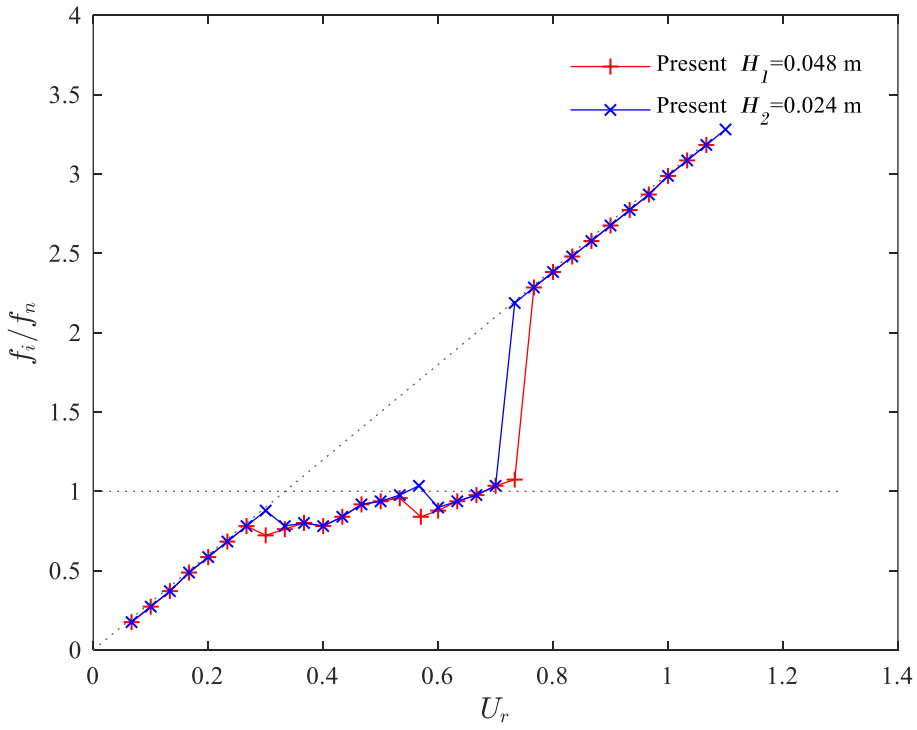

Figure 2.9. Reduced velocity vs. ratio between predominant ice force frequency $\boldsymbol{f_i}$ and structural natural frequency $\boldsymbol{f_n}$.

Accordingly, the predominant frequency of the structural response increases with the velocity till the lock-in range from to 0.22, as shown in Figure 2.10. Then, it fluctuates under the natural frequency of the structure following a similar trend with that in Figure 2.9, and stays at around the natural frequency afterwards. This relationship can also be confirmed from experimental results obtained by Määttänen (1983) and Tsuchiya et al. (1985), and numerical model result generated from Matlock et al. (1971) model. However, structural response frequency has not only its value, but also its corresponding response amplitude at the same time, indicating the structural response amplitude. The blue dash line in Figure 2.10 shows the relative amplitude difference (relative amplitude is based on the maximum response value at v = 0.2 m s^{-1}), from which it shows the structural response increasing at quasi-static region then vibrating at high response as well as reaching the maximum during steady-state range. As the velocity increases further, frequency value stays at around the natural frequency while the response amplitude is decreasing to almost zero, which can also be verified from Huang et al. (2007).

According to the frequency value and response, the structural response locks in to the natural frequency at around 0.08 m s^{-1} to 0.22 m s^{-1}, which has a slightly difference from the lock-in range in Figure 2.9. To be consistent with the original theory, the lock-in range in the context is defined by using ice force frequency, i.e. values from Figure 2.9.

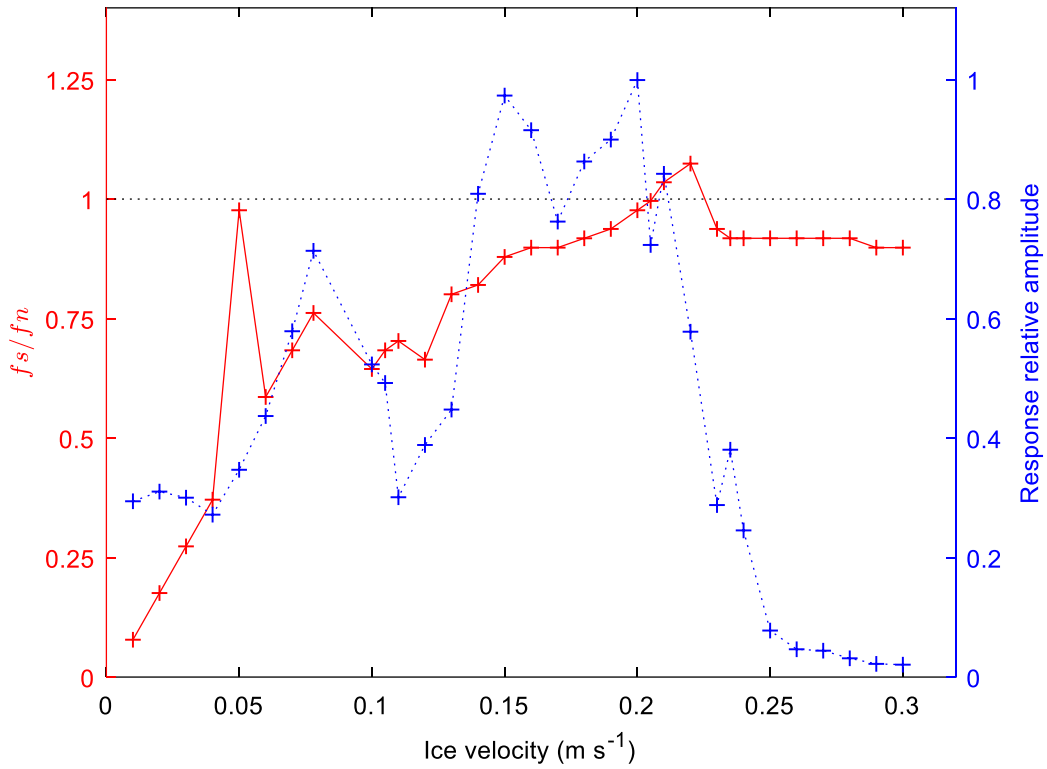

Figure 2.10. Ice velocity vs. ratio between predominant structural response frequency $\boldsymbol{f_s}$ and structural natural frequency $\boldsymbol{f_n}$ at $\boldsymbol{H_1}$ =0.048 m.

2.6 Summary

In this chapter, the physical mechanism in ice-induced vibrations between forced vibration and self-excited vibration and the similarity between ice-induced vibrations and vortex-induced vibrations are discussed. On the basis of ice behaviour observed in full and small-scale experiments, a novel dynamic ice-structure interaction numerical model is developed considering ice stress variations as well as its internal and external effects. Results show good agreements with that in full and small-scale experiments and that in other numerical models, like Matlock et al. (1971) and Huang and Liu (2009), including structural velocity relationship with ice velocity, ice force and structural displacement profile for three distinct modes from low to high velocities, and the IIV phenomenon caused by ice force frequency lock-in.

CHAPTER

3. PHYSICAL MECHANISM OF ICE-STRUCTURE INTERACTION

3.1 Introduction

Even after around half a century, the basic physical mechanism of the severest vibrations during ice-structure interaction, IIV, is still not fully understood. Blenkarn (1970) and Määttänen (2015) argued that it was the reason of self-excited vibration because of the negative damping theory. On the other hand, Sodhi has forced vibration from resonance opinion as in Sodhi (1988) because negative damping explanation is not rigorous. Besides, Sodhi (1991a) found that energy is always dissipating into ice, which rules out the chance of negative damping to occur.

In this chapter, before providing further explanations of ice mechanics, an extension of Ji and Oterkus (2016) model will be introduced first. This model is based on substituting an empirical parameter c_0 in Eq. (2.6) to include structural stiffness and ice velocity effects. Then, a series of reproduced numerical results based on the experiments done by Sodhi (1991b) will be presented. Finally, physical mechanism of ice-structure interaction process and ice force frequency lock-in during IIV will be discussed from both Määttänen and Sodhi's point of view by analysing negative damping phenomena, energy exchanges and stress variations based on reproduced numerical results.

3.2 Model description

3.2.1 Ice failure length

Ice failure length is an idealised concept for numerical calculation based on the damage zone or crushing zone concept in experimental tests. Ice failure length is taken as a constant 1/3 of ice thickness in Ji and Oterkus (2016), which means ice fails at a certain length if ice thickness does not vary. However, it ranges from 1/2 to 1/5 of ice thickness according to the tests by Sodhi and Morris (1986) covering an area when it is used for ice force predominant frequency calculations. It is the reason that ice damage zone becomes smaller by increasing ice velocity (Kry, 1981; Sodhi, 1998). At low ice velocity, there is a large damage zone with radial cracks along from the contact area.

When the velocity reaches high level, the damage zone becomes much smaller with only micro cracks near the interaction surface.

Sodhi (1998) proposed another concept, i.e. correlation length parameter L, to describe the size and the amount of damage zone of ice in relation to ice velocity. He proposed an equation to estimate this parameter in the form of $L/H = (v_0/v)(d/H)$, where v_0 is a reference velocity, $d = D/n$ is the segment width, n is the number of segments used as 1, 3, 5 or 7 to control the structural width D, and d/H ratio is in the 1-3 range. It can be seen that the correlation length is decreasing with increasing ice velocity. In this paper, structural width is considered as one whole segment, i.e. $n = 1$. Thus, the equation is used in the form of $L/H = (v_0/v)(D/H)$. Assuming $D/H = 2$, then $L/H = 2v_0/v$ which is done under the assumption that the ice failure length has a relationship to ice thickness and not to structural width (Sodhi, 1998).

In addition to ice velocity, ice force frequency is proportional to structural stiffness (Määttanen, 1975; Sodhi and Nakazawa, 1990). Experimental tests conducted by Sodhi (1991b) also show this relationship. These are Test 63, Test 66 and Test 67 under almost the same conditions except that the structural stiffness in each test was 3230, 1710 and 890 kN m^{-1}, respectively. Time-history plotting of ice force in Sodhi (1991b) showed that the average maximum value was around 15 kN in all tests. However, the frequency showed an approximately linearly decreasing trend when the structural stiffness decreases, with the value of 3.33 Hz, 2.17 Hz and 1.25 Hz, respectively.

Since ice force frequency is determined by the ice failure length parameter, it is assumed that ice failure length is inversely proportional to structural stiffness. Following the effect of ice velocity on ice failure from correlation length parameter and by adding up the linear structural stiffness effect, the general form of ice failure length can be written as

$$\frac{L}{H} = 2\frac{v_0}{v}\frac{K_0}{K} \tag{3.1}$$

where K_0 is the reference structural stiffness and K is the structural stiffness. Constant value of 2 also satisfies the ratio of structural width to ice thickness in the range of 1.67 and 2.08 as listed in Table 3.1. If the mass of the structure remains the same, the natural frequency of the structure will be proportional to the structural stiffness as

$\omega_n = \sqrt{K/M}$, where ω_n is the angular natural frequency of the structure and M is the mass of the structure. Besides, the ISO 19906:2010 tends to use the structural natural frequency to define the highest ice velocity that lock-in condition can occur, $v = \gamma_v f_n$, where $\gamma_v = 0.06\,m$. Hence, Eq. (3.1) can be rewritten in the form of

$$L = 2H \frac{v_0}{v} \frac{f_0}{f_n} \tag{3.2}$$

by substituting the stiffness with the frequency, where f_0 is the reference frequency and f_n is the natural frequency of the structure.

3.2.2 Main equations

In this study, governing equations and ice stress-strain rate relationship are adopted directly from Ji and Oterkus (2016). Unlike the experiment done by Sodhi (1991b) in which an indenter is pushed through ice sheet, in the current numerical model ice is moving against a stationary structure.

3.2.3 Parameter values

Most of parameters in the Eq. (2.5) and (2.7) are determined from the tests conducted by Sodhi (1991b) and summarised in Table 3.1. In the equation of motion, $A = 0.22$ is the magnification factor adjusted by Test. 63 to match the upper bound of the ice force from the tests except for the Test. 110 which is 0.15. $a = 2$ is set to assume that all force will drop to zero after each cycle of loading. $D = 0.05$ m and $M = 600$ kg are from the test configuration. $\xi = 0.1$ is not given but found in Figure 5 of Sodhi (1994). In the Van der Pol equation, $\varepsilon = 4.6$ is adjusted for better force envelope behaviour. $B = 0.1$ is calibrated by the results from Test. 63 and Test. 67. In the ice stress-strain rate equation, σ_d=8800 kPa because the maximum pressure is 8.8 MPa from Test. 64. In Test. 66, the effective failure pressure varies from 8-13 MPa under intermittent crushing. Therefore, σ_{max}=13000 kPa is used for maximum value and $\alpha = 0.35$. In Test. 67, the pressure is 4.4 MPa. Therefore, σ_b=4400 kPa and $\beta = -6$ except for Test. 203 at high velocity, i.e. σ_b=1700 kPa from the data provided. Transition ice velocity is set to v_t =0.05 m s^{-1} because high velocity range described by Sodhi was above 0.1 m s^{-1} and the middle value is estimated. In the ice failure length equation, v_0 =0.03 m s^{-1} is used as suggested by Sodhi (1998). K_0 =710 kN m^{-1}, i.e.

f_0 =5.47 Hz, is adjusted by the results from Test. 63 and Test. 67. Summary of all parameter values is listed below:

$D = 0.05$ m, $M = 600$ kg, $\xi = 0.1$, $A = 0.22$ (0.15 for Test.110), $a = 2$;

$\varepsilon = 4.6$, B = 0.1, $v_0 = 0.03$ m s^{-1}, $K_0 = 710$ kN m^{-1}, $f_0 = 5.47$ Hz;

$\sigma_d = 8800$ kPa, $\sigma_b = 4300$ kPa (1700 kPa for Test. 203), $\sigma_{\max} = 13000$ kPa,

$\alpha = 0.35$, $\beta = -6$, $v_t = 0.05$ m s^{-1}.

Table 3.1. Test configurations from Sodhi (1991b)

Test No.	Ice velocity (m s^{-1})	Ice thickness (m)	Structural stiffness (kN m^{-1})	Structural natural frequency (Hz)	Structural width (m)	Fig. No. in Sodhi (1991b)
63	0.0411	0.027	3230	11.68	0.05	Fig. 3a
66	0.0411	0.0275	1710	8.50	0.05	Fig. 2b
67	0.0412	0.027	890	6.13	0.05	Fig. 3b
110	0.1031	0.03	2700	10.68	0.05	Fig. 5
203	0.1452	0.024	1130	6.91	0.05	Fig. 2c

3.3 Results

Based on the experimental results, reproduced results generated from the numerical model are shown in Figure 3.1, which are in a pretty good match with those from experiments. In these figures, records of variables are plotted with respect to time, such as ice force, displacement of the structure, acceleration of the structure and structural displacement with respect to the ice. Relative displacement is calculated by subtracting the structural displacement from ice displacement. Positive direction of the structural motion, i.e. the same direction as ice motion, is in the opposite direction with respect to Sodhi's results since the ice is assumed to move against the structure in the model whereas the indenter is set to move against the ice sheet in the Sodhi's experiments.

Figure 3.1 (a), (b) and (c) show results for Test. 63, Test. 66 and Test. 67, respectively, where all parameters are the same apart from the structural stiffness. The values of stiffness are 3230, 1710 and 890 kN m^{-1}, respectively. Amplitude and frequency of ice force and displacement are almost the same as those in experiments, reaching at 15 kN, with around fourteen, eight and five cycles of ice loading in four seconds, respectively. Although the ice failure forces are approximately the same, the ice failure frequency

in each figure shows a clear dependence on the stiffness, because structural stiffness has a linear relationship with ice failure length as controlled by Eq. (3.1).

Acceleration in Figure 3.1(a) shows around fifty percent bigger than that in the test (see Figure 3 (a) in Sodhi (1991b)) because there are some drops during loading phases. Moreover, there are some drops around the peak values, which are realistic since the stress varies with the relative velocity. When the force reaches the maximum, the relative velocity will become zero leading the force to drop to the corresponding stress value. In addition, this difference may be the reason of filtering process in experimental data that eliminates some sharp peak fluctuations and lowers the acceleration amplitude significantly.

If we take the Figure 3.1 (c) as an example in which force and displacement are plotted more clearly, there is almost no acceleration of the structure during loading phase in the detailed plot. At the instant of ice failure, the structure is in the maximum excursion place and the potential energy stored in the spring is then transformed into kinetic energy, moving the structure backwards against ice motion. The interaction force then drops to a much lower level suddenly at around 1/3 of the value at the instant of failure. It is the reason that crushed ice is in contact with and extruded by the backwards motion of the structure. After the extrusion, ice lost contact with the structure for a short time while the force is almost zero, which is called as separation phase according to Sodhi.

In Figure 3.1 (a) and (b), it can be noticed that there are some sudden unloading of ice force before it reaches to the maximum, which also cases a second order of periodicity in ice force and structural response. It occurs because of the external structural effect when the structure is moving backwards with respect to ice motion at first. The compressive stress between ice and structure results in ice deformation and failure occurs when the deformation exceeds the natural ice failure length L can tolerate. So, relative displacement is subtracted by the amount of L additionally leading to a negative value. Moreover, this external effect occurs after three cycles of loading in Figure 3.1 (a) and four cycles in Figure 3.1 (b), respectively. Due to the space limit, simulations are all run in sixteen seconds but plotted in four seconds only. The reason that there is no such external effect in Test No. 67 is because structural stiffness, i.e. structural natural frequency, has an impact on the lock-in condition range as the ISO

19906:2010 revealed. As defined in Eq. (3.2), the higher the structural stiffness, the smaller the ice failure length. Therefore, lock-in condition will occur even under the same ice velocity if structural stiffness is high enough.

Figure 3.1 (d) shows a steady-state vibration of the structure with a frequency close to its natural frequency. The ice force shows almost exactly the same periodic "spike" like loading envelope profile as that in the test, in which the maximum amplitude of force is around 11 kN and a frequency of 9 Hz approximately. It can be noticed that range and amplitude of structural displacement and acceleration are different from those in the test. There are two reasons for this difference because of ice force. The first reason is that ice force is controlled to drop to zero during each cycle of loading. The second is only the maximum value is considered and predicted. Similar difference can also be found in Figure 3.1 (e), which shows the continuous crushing behaviour under high ice velocity. Ice force is matching at around 2.5 kN with the test and no obvious vibration of the structure is found.

However, there is an obvious limitation in this model in which ice force always drops back to zero after every failure cycle. As shown in a series of tests in Sodhi (1991b), ice force drops back to zero only at relatively low indentation speed, such as $v = 0.0412$ m s^{-1} in Test. 63. Then, as the speed increases, such as $v = 0.1031$ m s^{-1} in Test. 110, some ice force draw back to zero but some drops back to a lower value. Then ice force does not drop back to zero at all at higher velocity, such as $v = 0.1452$ m s^{-1} in Test. 203. It is due to the fact that ice fails non-simultaneously at the interaction surface between ice and structure leaving a certain level of force to structure. This remaining force is also the constant force added to the original Matlock model in Coburn et al. (1984).

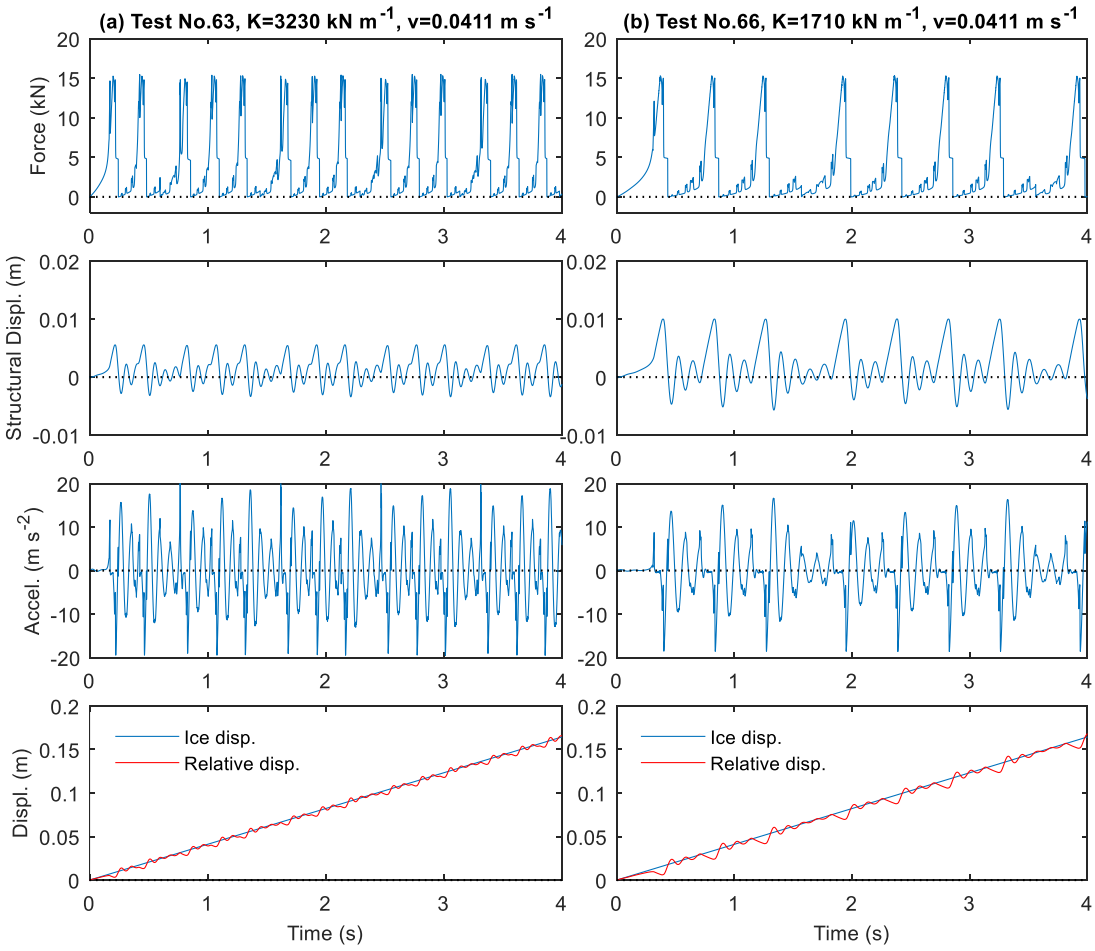

Figure 3.1. (a).

Figure 3.1. (b).

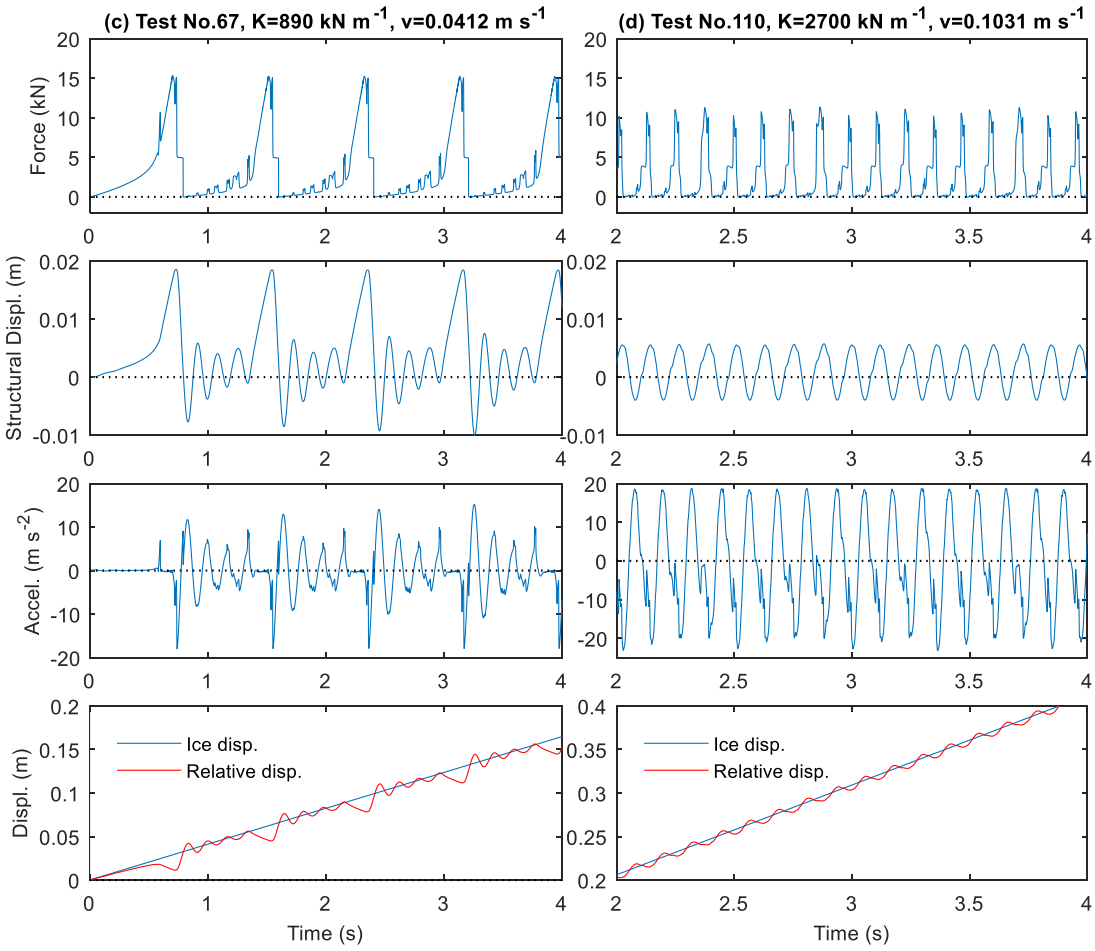

Figure 3.1. (c).

Figure 3.1. (d).

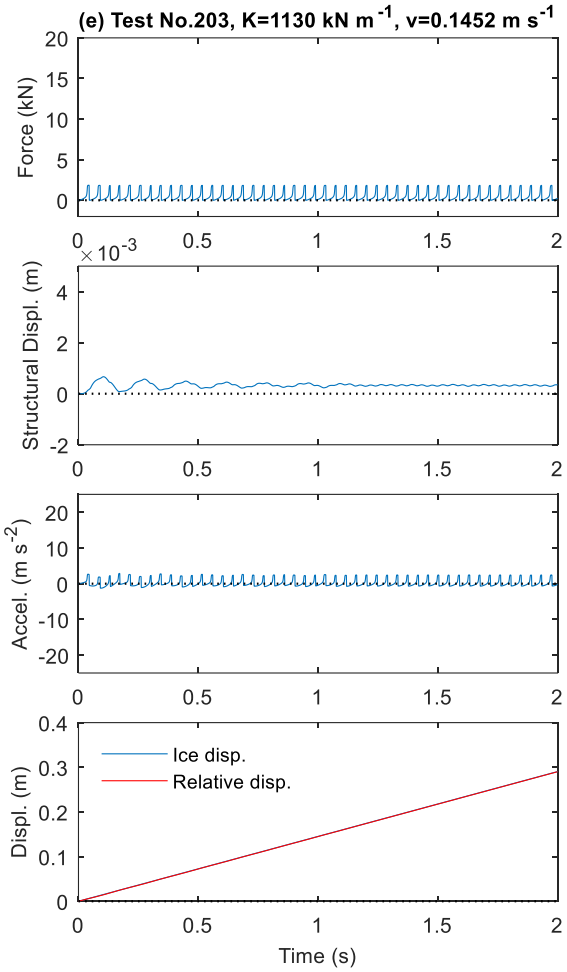

Figure 3.1. (e).

Figure 3.1. Time history of ice force, structural displacement, acceleration, and ice displacement with relative displacement at different structural stiffnesses and ice velocities. (a) Test. 63, K=3230 kN m^{-1}, v=0.0411 m s^{-1}. (b) Test. 66, K=1710 kN m^{-1}, v=0.0411 m s^{-1}. (c) Test. 67, K=890 kN m^{-1}, v=0.0412 m s^{-1}. (d) Test. 110, K=2700 kN m^{-1}, v=0.1031 m s^{-1}. (e) Test. 203, K=1130 kN m^{-1}, v=0.1452 m s^{-1}.

3.4 Physical mechanism

According to the definition from Den Hartog (1947):

- In self-excited vibration, the alternating force that sustains the motion is created or controlled by the motion itself. When the motion stops, the alternating force disappears.
- In forced vibration, the sustaining alternating force exists independently apart from the motion and persists even when the vibratory motion is stopped.

Sodhi (1988) discussed ice-induced vibrations as forced vibration because ice force persists when the structure is prevented from moving. However, it is a fact that ice failed at a certain amount with certain frequency (Kärnä et al., 1993; Neill, 1976; Sodhi, 2001; Sodhi and Morris, 1986). So, the situation will be different if the analysis of ice failure process is restricted to just one single failure cycle, when there is no feedback coming from the structure. There is a time interval after the first amount of ice fails and before another piece of ice approaches, which is a process for ice fragments to be removed. Both Sodhi (1988) and Määttänen (2015) pointed out this process and named "clearing process" and "gap", respectively, since ice force will vanish if the structure is stopped from moving. Therefore, it is not a forced vibration but self-excited vibration in this situation.

Depending on the number of ice elements in the system of interest, these two mechanisms can be converted. A similar statement can also be found in Ding (2012). If the studied system is extended to a macro scale, the external excitation caused forced vibration will be converted into the internal excitation that leads to self-excitation vibration, and vice versa. Taking ice as an example, if the ice and structure are coupled as one dynamic system, the IIV should belong to self-excited vibration category. On the contrary, if the structure is isolated from the ice and is considered as one dynamic system, the fluctuating force caused by ice failure would be an external excitation and IIV should be categorised as forced vibration. Therefore, there are internal and external effects from the structure point of view.

From the ice point of view, there are internal and external effects too. Internal from ice is the original ice failure characteristic. It is the behaviour under the assumption that ice fails against a theoretically rigid structure, which means there is no vibration or feedback coming from the external structure. But structure does vibrate in real cases. Hence, the structural vibration or oscillation effect is the external effect to the ice failure. Back in numerical modelling, the external effect is represented in the stress variations and the forcing term on the right-hand side of Van der Pol equation. If the stress is a constant and the forcing term is zero, then ice will fail under purely internal effect. Otherwise, relative velocity and relative displacement from structure will be effective in ice failure and lead to different ice force and structural movement behaviours, i.e., the general three responses shown in the Figure 3.1(c), (d) and (e).

Further explanations can also be given from the ice point of view in analysing ice failure. If the ice velocity is slow, ice force will drop to almost zero after each failure which means that time interval for clearing process is relatively long. If the velocity increases, the time interval will consequently become shorter. At the intermediate velocity range, ice fails under the structural oscillation effect besides the original failure nature which means that when the structure moves backwards against the ice, compressive stress arises due to external structure feedback and leads to ice deformation and failure more predominantly.

3.4.1 Reasons of lock-in

Even though ice force frequency tends to increase with increasing ice velocity, it still locks in around the structural natural frequency because of the external structural oscillation feedback effect and related stress variations. The change of stress depends on the strain, i.e. relative velocity between ice and structure. When the structure and ice move in the same direction during IIV, the relative velocity is low and the value of stress is high. The increasing ice resistance decelerates the structure moving with respect to ice and results in ice failure frequency lagging behind the originally supposed frequency if the structure is considered as rigid without vibration. The lagging frequency is called hysteresis frequency. Once ice failure occurs, ice and structure start moving in opposite directions and the relative velocity becomes high. Hence, low ice stress value reduces the ice resistance and accelerates the structure backwards against ice (Määttänen, 2015) exerting much lower ice force value upon the structure. More ice element failures result in higher ice force frequency than the originally supposed frequency. At the same time, during each interaction with the structure the oncoming ice sheet will also decelerate the structural velocity and raise the stress value because of lower relative velocity. Once the structural deceleration and acceleration oscillation process are in a stable feedback condition when restoring force is equal to the ice force, the structure will be in a self-excited oscillation condition. Therefore, the structural natural frequency will be predominant of the oscillation and ice force predominant frequency locks in the structural natural frequency.

When ice velocities are above the IIV lock-in range, relative velocity will stay at higher range resulting in very small-time interval for the structure to give feedback to ice. Consequently, ice original failure characteristic becomes predominant and ice force

frequency will increase with increasing ice velocity. At the same time, the response amplitude is decreasing with lower ice stress leading to the structure vibrating at a natural frequency with small amplitude or even diminishes (Huang et al., 2007).

3.4.2 Damping

Damping cannot be neglected when the structure is oscillating, especially in IIV. Yue and Guo (2011) and Kärnä et al. (2013) noticed that vibrating frequencies during IIV are slightly below the natural frequency. It is the reason when damping force is large compared to the spring or inertia forces that differ from the natural frequency appreciably (Den Hartog, 1947).

Mathematically, self-excited vibration occurs when there is an equilibrium between damping energy and external excitation energy during a full cycle of vibration (Ding, 2012) so that the structure vibrates by itself without input from external excitation energy to the mechanical system. In other words, the excitation energy is totally dissipated by damping, i.e. zero net input energy in a cycle of vibration. Therefore, an alternative way of understanding for this mechanism is by adding the negative damping to free vibration (Den Hartog, 1947). It is therefore called "self-excited" because there is no external excitation during a cycle of vibration.

Negative damping, in essence, is used as an external source of energy to increase the amplitude of vibration. As the characteristic of decreasing ice stress with increasing loading rate, Blenkarn (1970) proposed ice force as a function of relative velocity and explained the increased vibration amplitude in IIV as negative damping theory:

$$M\ddot{X} + C\dot{X} + KX = F(v - \dot{X}) \tag{3.3}$$

For small motions, forcing term can be written as:

$$F(v - \dot{X}) = F(v) - \dot{X}\,\frac{\partial F(v)}{\partial v} \tag{3.4}$$

Hence, Eq. (3.4) becomes:

$$M\ddot{X} + (C + \frac{\partial F}{\partial v})\dot{X} + KX = F(v) \tag{3.5}$$

Sodhi (1988) expressed some disagreement even though he thought negative damping was realistic under some conditions. General reason was that the forcing term was not only controlled by relative velocity but also relative displacement, time, etc. Therefore, a more detailed relationship between ice force and relative velocity needs to be

justified. Because of this reason relative displacement effect is also considered in the current numerical model during ice force calculation. As Sodhi mentioned, a plot of ice force vs. relative velocity can be more persuasive. For instance, Figure 3.2 is the result from Test. 110 in which ice force can be taken as a function of relative velocity. It is clear that the slope, $\partial \mathrm{F}/\,\partial v_r$, is sometimes positive and sometimes negative. The negative value can lead to net negative damping in Eq. (3.5) which will then lead the system to unstable condition. The blue line is the first cycle of loading which has higher negative slope comparing with other stable conditions such as the red line in a cycle of "spike" like ice loading under steady-state vibration and others in black dashed lines.

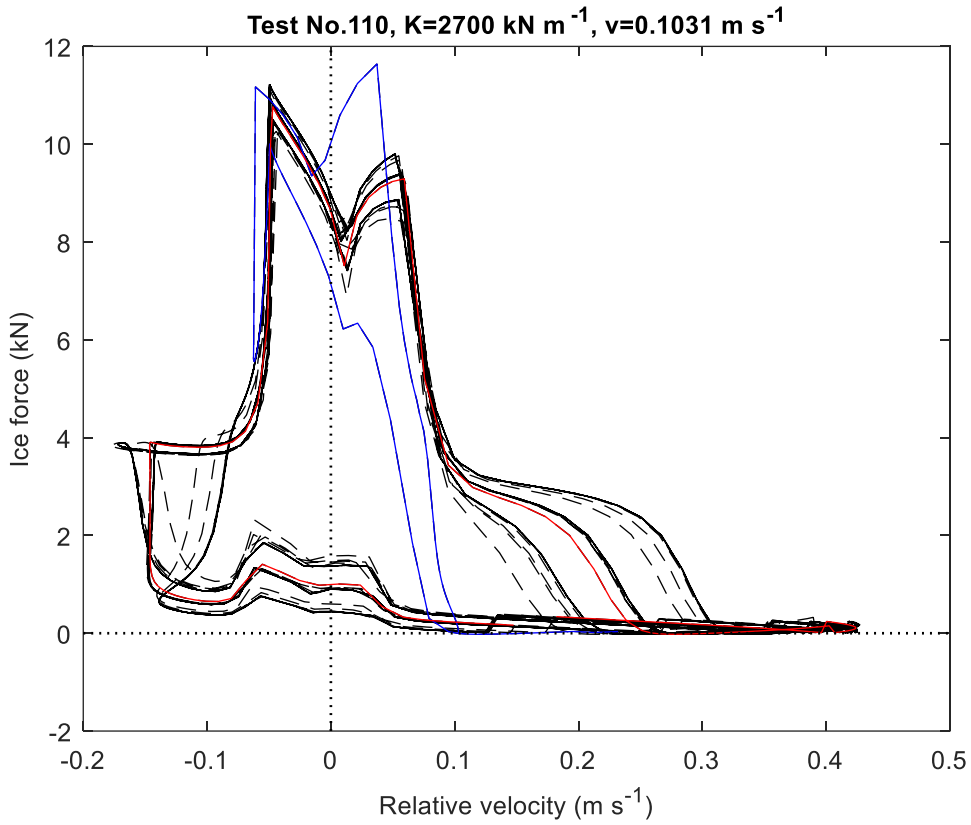

Figure 3.2. Relative velocity vs. ice force in four seconds (black dashed): the first cycle of loading (blue) and "spike" like loading (red).

3.4.3 Energy conservation

It is certain that energy is always conservative during ice-structure interaction process. The ultimate reason of increased structural vibration is due to more net energy input to structure. Force increases when "negative damping" occurs and more energy

transmits into the structure leading to increased vibration amplitude (Den Hartog, 1947). Note that the negative damping proposed by Blenkarn (1970) is actually moving the external structural velocity related forcing term from the right-hand side of the equation of motion to the left-hand side.

Sodhi (1991a) presented further evidence that there is no real negative damping based on his experimental results given in Sodhi (1991b). Instead, he found that the cumulative work done by the indenter is a non-decreasing function. According to the first law of thermodynamics, frictional and damping force of the structure are always dissipating energy into heat. Therefore, a positive damping force does negative work. In the present model, the energy relationship satisfies the following equation during the interaction process:

$$\Delta W_t = \Delta E_m + \Delta E_d \tag{3.6}$$

where ΔW_t is the incremental work done by ice, ΔE_m is the incremental change of mechanical energy in the structure and ΔE_d is the incremental heat dissipated by the structural damping since friction between ice and structure is not considered in the model. The incremental change of mechanical energy in the structure can be written as

$$\Delta E_m = \Delta E_p + \Delta E_k \tag{3.7}$$

where ΔE_p and ΔE_k are the incremental change of potential energy and kinetic energy in the structure, respectively. The computation of ΔW_t between any two instants of time is through multiplying the average force by the corresponding incremental structural displacement, i.e. $\overline{F}\Delta X$. The change of kinetic energy and potential energy are obtained from $0.5M\Delta\dot{X}^2$ and $0.5K\Delta X^2$, respectively. The energy dissipated due to damping can be computed from Eq. (3.6). The cumulative form and integral form of Eq. (3.6) and (3.7) are

$$\Sigma\Delta W_t = PE + KE + \Sigma\Delta E_d \tag{3.8}$$

$$\int_0^T \overline{F} dX = \int_0^T KX dX + \int_0^T M\dot{X} d\dot{X} + \int_0^T dE_d \tag{3.9}$$

Each parameter in Eq. (3.8) is shown in Figure 3.3 at four different tests such as total cumulative energy done by ice force ($\Sigma\Delta W_t$) in red, potential energy (PE) in purple, kinetic energy (KE) in green, mechanical energy of the structure ($PE + KE$) in black, and dissipated energy due to damping ($\Sigma\Delta E_d$) in blue. It can be noticed that most of

the energy arises from ice force dissipated by the damping of structure which is different from what Sodhi (1991a) found, i.e. energy supplied by carriage was dissipated mostly by the indenter. Because in the tests of Sodhi (1991b), an indenter, i.e. structure, was attached to a carriage to move against the ice in a basin. To simplify the modelling and understanding, ice is moving towards the structure in the current numerical model. Therefore, subtracting the work done by carriage from indenter in the experiment is the same work done by the ice force in the present model.

According to the numerical results, there are three different energy exchange characteristics because of three different types of ice-structure interactions at different ice velocities which capture the general similar pattern with those in Sodhi (1991a). Figure 3.3(a) and (b) show the failure under intermittent crushing. During each cycle of loading, the structure moves with the increasing force, resulting in large displacement but relatively small velocity of the structure. Energy supplied by ice is mostly stored in the structural spring. After the failure of ice, the stored potential energy is then transferred to kinetic energy leading to the backwards movement of the structure and extrusion of ice. Damping mechanism consumes the energy all the time when the velocity of the structure increases and reaches a balance condition with the energy from ice force at the end of each cycle of ice failure. Figure 3.3(c) shows the energy exchange at steady-state vibration. From the enlarged detail of the dashed box, it can be seen that potential and kinetic energy are in a sinusoidal exchange relationship similar to what Sodhi (1991a) found. After first few cycles of loading, the energy supplied by ice force in one cycle is equal to the energy dissipated by the damping. During the continuous crushing at high velocity, as shown in Figure 3.3(d), most of the mechanical energy are in the form of potential energy remaining at around a constant and kinetic energy remains at almost zero. Because the structure is pushed by ice to a relatively static position, it vibrates at much lower amplitude.

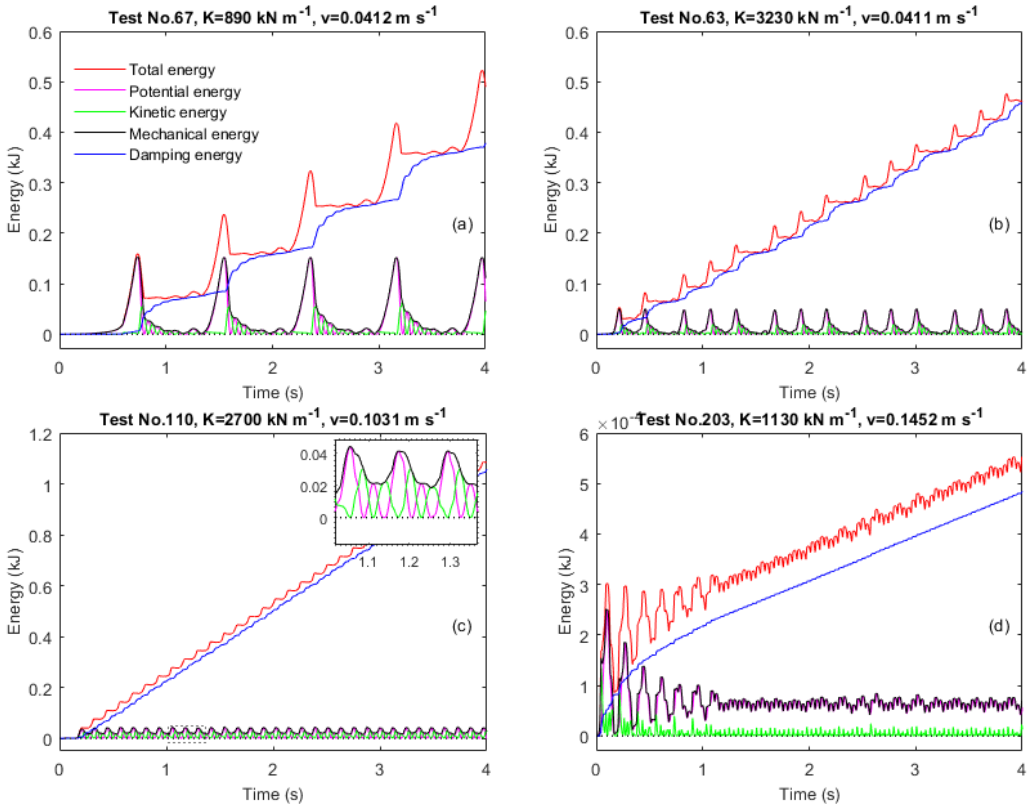

Figure 3.3. Time vs. total energy (red), potential energy (purple), kinetic energy (green), mechanical energy (black) and damping energy (blue) at different test configurations. (a) Test. 67, K=890 kN m^{-1}, v=0.0412 m s^{-1}. (b) Test. 63, K=3230 kN m^{-1}, v=0.0411 m s^{-1}. (c) Test. 110, K=2700 kN m^{-1}, v=0.1031 m s^{-1}. (d) Test. 203, K=1130 kN m^{-1}, v=0.1452 m s^{-1}.

3.4.4 Stress and force variations

Since 0.0412 m s^{-1} and 0.1452 m s^{-1} in Sodhi (1991b) was defined as intermediate and high velocity, respectively, estimated range of ice velocity at the test condition is between 0.01 m s^{-1} and 0.165 m s^{-1} approximately. Five sets of tests for the configurations in Table 3.1 were conducted except that ice velocities were used from 0.01 m s^{-1} to 0.165 m s^{-1} at 0.005 m s^{-1} intervals. Histograms of time history plotting of stress values and ice force values in each set of tests show similar pattern with each other as the ice velocity increases. Two sets of tests, Test. 67 and Test. 110, are chosen as shown in Figure 3.4(a) and (b), respectively. During each 0.005 m s^{-1} ice velocity, time history plotting of stress and ice force points are counted and accumulated at 0.725 MPa and 0.5 kN intervals, i.e. 0.3625 MPa and 0.25 kN from both sides of each

histogram, respectively. Ranges of stress and force are determined by the minimum and maximum values of them. Each histogram amplitude is then normalized into the relative amplitude by the maximum accumulated amplitude in each set of tests. Stress variations show a trend from low velocity high stress to high velocity low stress. Ice force variations show a concentration at around intermediate velocities range, i.e. IIV range, which means there is more integral of force over the same time interval, i.e. impulse energy, applied to increase the momentum of the structure. This situation occurs at the condition when stress values are relatively evenly distributed. These patterns may be worthwhile to be noticed from an energy conservation point of view.

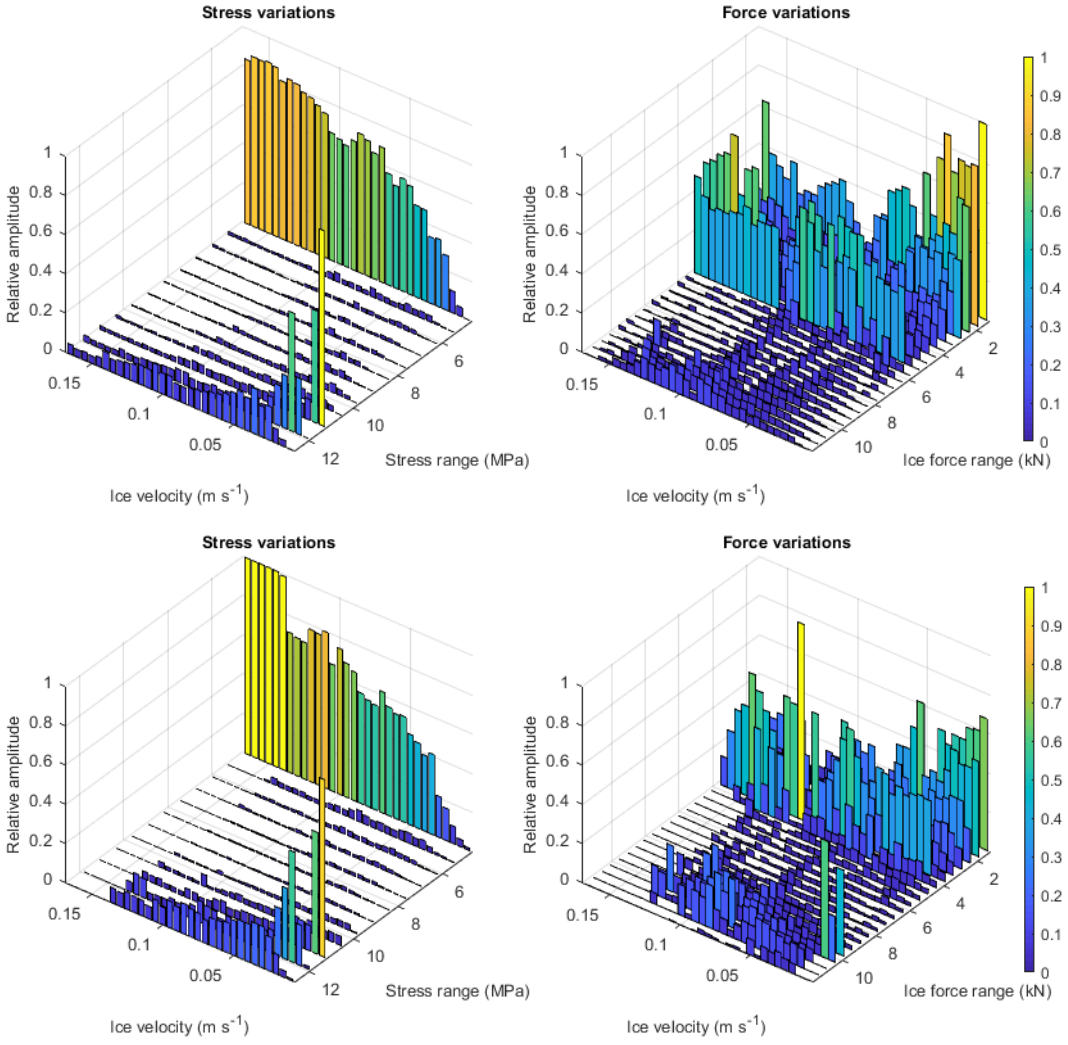

Figure 3.4. Histogram of stress and ice force variations at different ice velocities. (a) Test. 67, K=890 kN m^{-1}, (b) Test. 110, K=2700 kN m^{-1}.

3.4.5 Type of vibration

It is debatable that whether IIV is forced vibration from resonance or self-excited vibration from negative damping as introduced earlier. One thing is certain that forced vibration does not need an initial condition. However, self-excited vibration needs to be trigged by forced vibration and it needs energy from an external source to sustain (Den Hartog, 1947).

No matter which type of vibration, both of them has the following relationship, $f_i = f_s = f_n$, in which frequency of ice force, structural displacement and structural natural frequency are all equal. Commonly speaking, resonance is a special type of forced vibration which occurs when the external excitation frequency is equal to the structural natural frequency. For instance, making one fork to vibrate first will cause another identical fork to automatically vibrate. So, it is controlled by the external source. If the excitation frequency is different from the structural natural frequency, resonance will disappear. On the other hand, in self-excited vibration, vibrating frequency is equal to the natural frequency and the excitation force should be a function of the motion variables, such as displacement, velocity or acceleration (Rao, 2004).

In IIV, vibration is self-excited predominantly because feedback from external structure makes more effect on ice failure and ice will affect the structure in return, like lock-in phenomenon. The reason of the increased vibration amplitude can be explained by the "negative damping" theory in an alternative way by keeping in mind that the damping is not negative in reality. The increased vibration is attributed to more energy into the structure when there is higher ice force and the stress value is concentrated mainly in the higher range of stress values.

For vibrations below and above the IIV range, structure vibrates at forced vibration mechanism predominantly because the time interval between each cycle of vibration is so short that there is no time for the structure to give feedback to ice. So, the internal ice failure characteristic makes more effect with lower stress and ice force.

3.4.6 Friction-induced vibration

Frictional force is another important effect that builds up the ice force characteristic. With the formation of micro cracks inside ice when it is interacting with structure, the static ice force is building up at the same time with the trend of sliding up and down motion along the vertical direction of interaction surface. Ice failure occurs when the

crack propagates till a certain level that cannot hold the force perpendicular to the interaction surface. At the same time, the maximum static frictional force along the vertical direction of interaction surface is reached.

After the failure, ice force shows a typical transition instant from static friction to kinetic friction, which can be found at all ice velocity ranges in the tests from Sodhi (1991a), such as the creep deformation at very low ice velocity in Test. 64, the extrusion phase at intermittent crushing under intermediate velocity in Test. 204 and transition from intermittent crushing to continuous crushing at high velocity in Test. 206.

Sodhi (1991b) found that effective pressure during continuous crushing is in an order of magnitude lower than the peak pressure during intermittent crushing from both full-scale and small-scale experiments. It can also be explained that kinetic friction occurs at higher velocities leading to much lower pressure. Sukhorukov (2013) found that the mean value of static and kinetic friction coefficients of ice on steel are 0.50 and 0.11 on dry surface, and 0.40 and 0.09 on wet condition, respectively, as shown in Table 3.2, where μ_s and μ_k are the static and kinetic friction coefficients, respectively. Although values of steel on ice have lower static friction coefficient, they are still much higher than the kinetic friction coefficients.

Table 3.2. Static and kinetic friction coefficients from ice-steel experiments (Sukhorukov, 2013).

Sliding configuration	Surface condition	μ_s	μ_k
Ice on steel	Dry	0.50 ± 0.12	0.11 ± 0.02
Ice on steel	Wet	0.40 ± 0.05	0.09 ± 0.02
Steel on ice	Dry	0.43 ± 0.09	0.12 ± 0.03
Steel on ice	Wet	0.36 ± 0.09	0.13 ± 0.04

Ice stress variations in IIV is very similar to frictional coefficient variations in friction-induced vibration when considering relative velocity only as shown in the three-region of Stribeck curve in Figure 3.5. A typical example is the self-excited vibration of a bowed violin string. The bow and string are moving in the same direction at first when the bow drags the string aside. The coefficient of friction is high because relative velocity is low and potential energy is storing in the string. When the maximum static

force cannot hold the restoring force from string, the string will slip back releasing the energy to kinetic energy in the form of backward velocity. The decrease in coefficient of friction yields lower frictional force, which will then accelerate the velocity further to a certain level. However, the coefficient will raise again due to the coefficient curve shown in Figure 3.5 and the system will be in a stable feedback condition when restoring force is equal to the frictional force. Less energy is lost than the input at first and the difference is enough to overcome the damping and sustain the vibration (Schmitz and Smith, 2011), like the energy exchange in steady-steady state shown in Figure 3.3 (c). The sound of vibrations is produced at its natural frequency since it determines the restoration of the string.

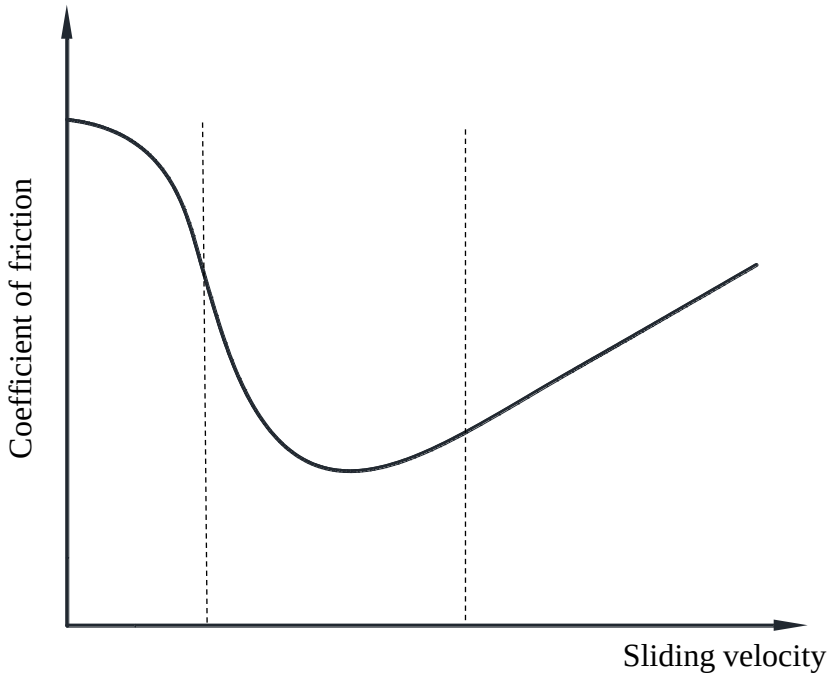

Figure 3.5. Stribeck curve.

3.5 Summary

To obtain the effect of velocity and structural natural frequency (structural stiffness) on ice failure, an extended model based on the previous work of (Ji and Oterkus, 2016) was developed. A series of validation cases were conducted and compared with the results from Sodhi (1991b) which show the typical three kinds of response; intermittent crushing, lock-in and continuous crushing and both numerical and experimental results are in good agreement with each other.

Physical mechanisms during ice-structure interaction process under different velocities were discussed based on the general branch of feedback mechanism and energy mechanism, respectively. Internal effect and external effect from ice and structure were both explained in the feedback branch. Energy exchanges of each type of energy were reproduced and coincided with analyses in Sodhi (1991a).

Reasons of the increased vibration amplitude during IIV and lock-in were presented and discussed starting from the disagreement between Sodhi and Määttänen and analyses were given from both perspectives. In addition, a study on the stress and force variations in full range of velocities showed that there was more impulse energy during IIV range which can be an explanation for the increased vibration amplitude from the energy point of view.

IIV is in a resonant type of self-excited vibration because the structural effect is more predominant. Even though negative damping is not negative in reality, it can be used to explain the self-excited vibration in an alternative way. A general conclusion on the predominant type of vibration during the interaction process is forced, self-excited and forced in each three types of responses.

Similar variations between ice stress and coefficient of friction shows that there is a likelihood to use static and kinetic friction force to explain the pressure difference at high and low velocities as well as the unstable and stable conditions during ice-induced vibrations.

An obvious limitation in this model is that ice force always drops back to zero after every failure. Therefore, to accurately simulate ice force characteristic at higher speed, non-simultaneous ice failure model is necessary.

CHAPTER

4. A NON-SIMULTANEOUS DYNAMIC ICE-STRUCTURE INTERACTION MODEL

4.1 Introduction

As the study of ice failure has advanced, non-simultaneous failure has gained increasing attention. It can be utilized to explain several well-recognized issues, such as higher localized pressure zone than global pressure (Johnston et al., 1998) and different failure modes at different indentation speeds (Sodhi and Haehnel, 2003). Kry (1978) proposed an estimation of statistical influence on non-simultaneous failure across a wide structure and divided the ice interaction surface into multiple equivalent zones that are statistically independent of each other. Then Kry (1980) found that ice generally had a more uniform contact with a structure at low velocity and more irregular contact at higher velocity. Ashby et al. (1986) explained the non-simultaneous failure as a size effect resulting from cracks of different lengths having been distributed statistically in ice. Bhat (1990) proposed that ice fails at many self-similar zones like many other fractals in nature and proposed an equation to control the size effect depending on the scale to estimate the irregular ice contact geometry.

Sodhi (1998) used segmented indentors to conduct a series of ice indentation tests and found simultaneous failure at low velocity and non-simultaneous at high velocity, and proposed an equation to estimate the decreasing size of ice failure length with increasing indentation velocity. Yue et al. (2009) installed ice load panel on a full-scale monopod platform and found simultaneous ice failure on different panels during lock-in condition.

At the same time, many ice-structure interaction numerical models have been developed. Matlock et al. (1971) proposed the very first ice-structure interaction model and many Matlock based numerical models have been developed since then (Huang and Liu, 2009; Karr et al., 1993; Withalm and Hoffmann, 2010). Non-simultaneous ice-structure interaction models have been developed based on Matlock model (Hendrikse et al., 2011; Yu and Karr, 2014) by extending the single ice strip into multiple strips moving towards the structure. Another method of modelling the

interaction process is through utilizing Van der Pol ice force oscillator to control ice force fluctuations (Wang and Xu, 1991). Three distinctive structural response modes and ice-induced vibration phenomenon were captured in Ji and Oterkus (2016). Physical mechanism of ice-structure interaction at each stage were discussed based on feedback mechanism and energy mechanism in Ji and Oterkus (2018).

In this study, following the concept of Matlock-based non-simultaneous modelling, an extension of Ji and Oterkus (2018) Van der Pol based model is introduced. Apart from the ice velocity and structural stiffness effect on the ice failure, the constant 2 in Eq. (3.2) from previous model is replaced with a normally distributed variable. In addition, the previous one-dimensional single strip ice model is extended to a two-dimensional multiple strips ice model in this study.

4.2 Experimental data from Sodhi (1998)

Sodhi (1998) listed 159 test results including structural width D, ice thickness H, ice velocity v, mean μ_p and standard deviation σ_p of the effective pressure across the interaction surface. In Test 582 and 576 as well as Test 764 and 763, they are sharing similar ice thickness and structural width but different ice velocities. In Test 582 and 764 as well as Test 576 and 763, they share similar velocities but different ice thicknesses and structural widths. Therefore, different tests, Test. 582, 576, 764 and 763, are simulated by the numerical model. The time history of ice force and structural displacement are plotted and compared with the time history of experimental results.

To use the data more efficiently for blind test later, they are relisted in Table 4.1. There are four main sections in total with different D ranging from 50 mm, 150 mm, 250 mm to 350 mm. Each section has several groups of data from (A) to (K). Each group has the ice thickness with 1 mm difference, or rarely with 1.5mm difference. Then each group is sorted from the lowest to the highest ice velocity. There are 25 tests that are not grouped together because of limited similar ice thickness, as shown in grey colour in Table 4.1. Therefore, 134 different tests are simulated by only changing the D, H and v. Then, μ_p and σ_p are compared between the numerical simulations and experimental results.

Table 4.1. Test configurations from Sodhi (1998).

Test	D mm	H mm	v mm s^{-1}	μ_p MPa	σ_p MPa	Group
166	50	25.1	62	2.032	0.243	
160	50	27.3	80	2.307	0.34	
165	50	24.8	100	2.12	0.224	
167	50	25	125	1.78	0.291	**(A)**
164	50	26.3	199	1.504	0.319	
163	50	25.6	300	1.644	0.256	
162	50	26.3	400	1.622	0.263	
161	50	25.7	492	1.915	0.301	
158	50	45.1	47	1.736	0.229	
154	50	44.4	82	1.681	0.229	
153	50	45.2	101	1.548	0.237	
155	50	44.2	127	1.877	0.265	
156	50	43.3	156	1.417	0.307	**(B)**
157	50	43.5	188	1.394	0.408	
152	50	45.6	197	1.461	0.188	
159	50	45.3	224	1.363	0.25	
151	50	43.9	304	1.392	0.247	
150	50	45.6	393	1.497	0.231	
175	50	69.7	103	2.491	0.555	
176	50	71.1	136	2.509	0.742	
362	150	15.3	406	2.405	0.275	
388	150	18.8	10	1.62	0.634	
387	150	18.8	20	0.806	0.25	
378	150	18.7	25	0.925	0.288	
386	150	18.5	31	1.086	0.306	
385	150	18.5	42	0.856	0.239	
377	150	18.7	42	0.986	0.287	
376	150	18.7	42	0.91	0.266	
373	150	17.3	52	1.012	0.192	**(C)**
375	150	17.6	74	1.055	0.192	
374	150	17.6	90	0.915	0.36	
375	150	17.6	99	1.144	0.199	
371	150	17.8	100	1.114	0.177	
372	150	17.8	200	1.263	0.171	
369	150	18.5	391	1.462	0.147	
370	150	18	394	1.399	0.167	
368	150	18.5	469	1.508	0.178	
384	150	19.2	21	0.991	0.331	
403	150	24.5	14	2.083	0.769	
402	150	24.5	21	1.657	0.724	
401	150	25.5	31	0.99	0.344	

Test	D mm	H mm	v mm s^{-1}	μ_p MPa	σ_p MPa	Group
399	150	25.5	44	0.933	0.3	
398	150	26.6	20	1.69	0.906	
391	150	27	20	1.907	0.862	
390	150	27	45	1.029	0.347	
410	150	30.6	20	1.869	0.831	
405	150	30	27	2.214	0.967	
411	150	30	43	1.077	0.321	
404	150	30	43	1.265	0.45	
356	150	32.3	81	1.402	0.4	
354	150	32.8	97	1.665	0.544	**(D)**
358	150	31.8	134	1.374	0.357	
357	150	32.4	134	1.372	0.287	
361	150	30.5	181	1.424	0.231	
359	150	31.2	187	1.178	0.245	
353	150	32.7	197	1.62	0.236	
351	150	33.3	395	2.06	0.197	
352	150	33.4	294	1.813	0.223	
366	150	45.1	194	1.706	0.38	
367	150	46	270	1.959	0.231	
364	150	46.2	197	1.819	0.45	
363	150	46.8	301	2.186	0.236	
534	250	17.9	48	0.803	0.287	
536	250	17.8	56	0.874	0.226	
535	250	17.7	72	0.864	0.207	
537	250	18.1	72	0.834	0.384	
538	250	17.9	73	0.917	0.167	
533	250	18	102	0.893	0.2	
521	250	18.2	149	0.997	0.13	**(E)**
532	250	18.1	201	1.026	0.184	
540	250	18.1	249	1.123	0.121	
531	250	18.2	300	1.158	0.212	
539	250	18.1	350	1.257	0.135	
549	250	18.5	355	1.234	0.13	
548	250	18.4	499	1.319	0.161	
516	250	24.8	10	1.58	0.948	
513	250	24.8	10	1.454	0.597	
528	250	25.4	21	1.536	0.791	
514	250	24.6	42	0.934	0.382	**(F)**
527	250	25.4	42	1.025	0.421	
592	250	23.6	83	0.937	0.253	
590	250	24.1	104	1.003	0.195	

Table 4.1. Continued

Test	D mm	H mm	v mm s^{-1}	μ_p MPa	σ_p MPa	Group
591	250	23.8	159	1.055	0.157	
589	250	23.9	202	1.141	0.131	
593	250	24	254	1.181	0.116	
588	250	24	315	1.212	0.132	**(F)**
587	250	24.5	373	1.246	0.121	
586	250	24.7	408	1.304	0.115	
585	250	25.1	465	1.377	0.124	
583	250	25.7	490	1.611	0.127	
582	250	32.7	102	0.961	0.288	
579	250	33.9	133	1.085	0.214	
578	250	33.3	199	1.199	0.162	
572	250	34.6	199	1.25	0.277	
581	250	33	246	1.236	0.146	**(G)**
577	250	34.2	312	1.291	0.141	
580	250	33	356	1.32	0.132	
575	250	33.2	386	1.436	0.131	
569	250	34.7	400	2.067	0.169	
576	250	33.9	409	1.383	0.129	
545	250	35.8	110	0.917	0.2	
596	250	35.1	200	1.194	0.169	
546	250	36.3	200	1	0.372	
544	250	35.6	215	1.065	0.147	
543	250	35.9	277	1.207	0.146	
547	250	36.8	298	1.238	0.362	**(H)**
595	250	35.4	301	1.41	0.17	
571	250	35.9	304	1.462	0.145	
542	250	35.5	331	1.332	0.145	
541	250	35.9	375	1.315	0.141	
594	250	35.5	399	1.581	0.182	
554	250	41.5	6	1.732	1.033	
555	250	42	6	1.572	1.419	
551	250	41.1	8	1.006	1.327	
559	250	40.4	145	1.197	0.29	
525	250	41.3	201	1.453	0.491	**(I)**
563	250	39.8	300	1.503	0.514	
524	250	40.9	304	1.77	0.256	
526	250	40.9	353	1.926	0.157	
523	250	39.8	392	2.112	0.179	
522	250	40.1	467	1.992	0.231	

Test	D mm	H mm	v mm s^{-1}	μ_p MPa	σ_p MPa	Group
556	250	42.2	6	1.258	0.807	
560	250	43.1	219	1.289	0.182	
553	250	44.3	8	1.198	0.819	
552	250	44.3	8	1.38	1.02	
760	350	20.3	82	0.835	0.143	
752	350	22.2	100	0.899	0.174	
759	350	20.2	156	0.939	0.088	
761	350	20.5	157	0.915	0.105	
755	350	20.7	172	0.994	0.094	
758	350	20.2	251	1.001	0.095	**(J)**
754	350	20.8	306	1.125	0.093	
757	350	20.3	354	1.117	0.085	
753	350	20.8	401	1.17	0.089	
751	350	21.1	453	1.214	0.09	
756	350	20.4	459	1.163	0.082	
771	350	24.5	80	0.859	0.263	
773	350	23.8	99	0.898	0.219	
777	350	24.5	99	1.121	0.298	
764	350	25.2	100	1.015	0.341	
779	350	24.8	115	1.067	0.278	
770	350	23.9	121	1.029	0.108	
780	350	24.8	150	1.223	0.217	
781	350	24.9	157	1.197	0.124	
782	350	25	193	1.23	0.122	
766	350	24.6	196	1.11	0.111	**(K)**
772	350	24	197	1.143	0.11	
776	350	24.5	199	1.272	0.133	
769	350	23.9	248	1.23	0.128	
775	350	24.7	277	1.547	0.123	
765	350	24.8	303	1.194	0.099	
768	350	24.4	350	1.264	0.099	
774	350	24.4	358	1.371	0.129	
767	350	24.4	452	1.297	0.105	
762	350	25.6	481	1.598	0.104	
763	350	26.4	401	1.405	0.105	
785	350	29.8	198	1.273	0.134	
784	350	30	305	1.624	0.129	
783	350	30.4	399	1.503	0.121	

To show the ice velocity effect on the ice force level, four groups of data, (C), (E), (F) and (J) at different structural widths with similar ice thicknesses are selected from Table 4.1, as shown in Figure 4.1. Figure 4.1 (a) and (b) show the mean μ_p and standard deviation σ_p of the effective pressure from Table 4.1, respectively. Figure 4.1 (c) and (d) are the maximum and minimum effective pressure calculated from $\mu_p \pm 2\sigma_p$, respectively. In Figure 4.1 (a) and (c), the pressure decreases from higher value to the lowest value first before ice velocity reaches the transition ice velocity. Reason of this pressure difference can be the difference between static frictional force at low velocity and kinetic frictional force at high velocity (Ji and Oterkus, 2018). After the transition ice velocity, the mean value increases approximately linearly with increasing ice velocity. It is due to the fact that there is more momentum energy transferred to the structure from ice, i.e. higher acceleration of the structure in the form of $F = M(\partial v/\partial T)$. Apart from ice speed effect, it shows that thicker ice has higher effective pressure and wider structure has lower effective pressure. In other words, the higher the aspect ratio of structural width D over ice thickness H, the lower the effective pressure is.

Figure 4.1 (b) shows the standard deviation of pressure decreases with increasing velocity. The decreasing trend indicates smaller ice failure size and the occurrence of more non-simultaneous failure. Provided that the minimum effective pressure to be $\mu_p - 2\sigma_p$, Figure 4.1 (d) also indicates that it has more dependency on ice velocity and less dependency on structural width or ice thickness. Slope at lower velocity is higher since simultaneous failure has large standard deviation caused by the maximum force value. For the same reason, the data points at lower velocity calculated in this method have less accuracy. Because there should not be any of negative pressure. Then the minimum value increases approximately linearly with ice velocity, which means that the lower bound of ice force follows the similar pattern. Considering that most part of the ice maintains constant contact with structure at high ice speed after failure, ice force will not reduce back to zero as that at lower ice speed.

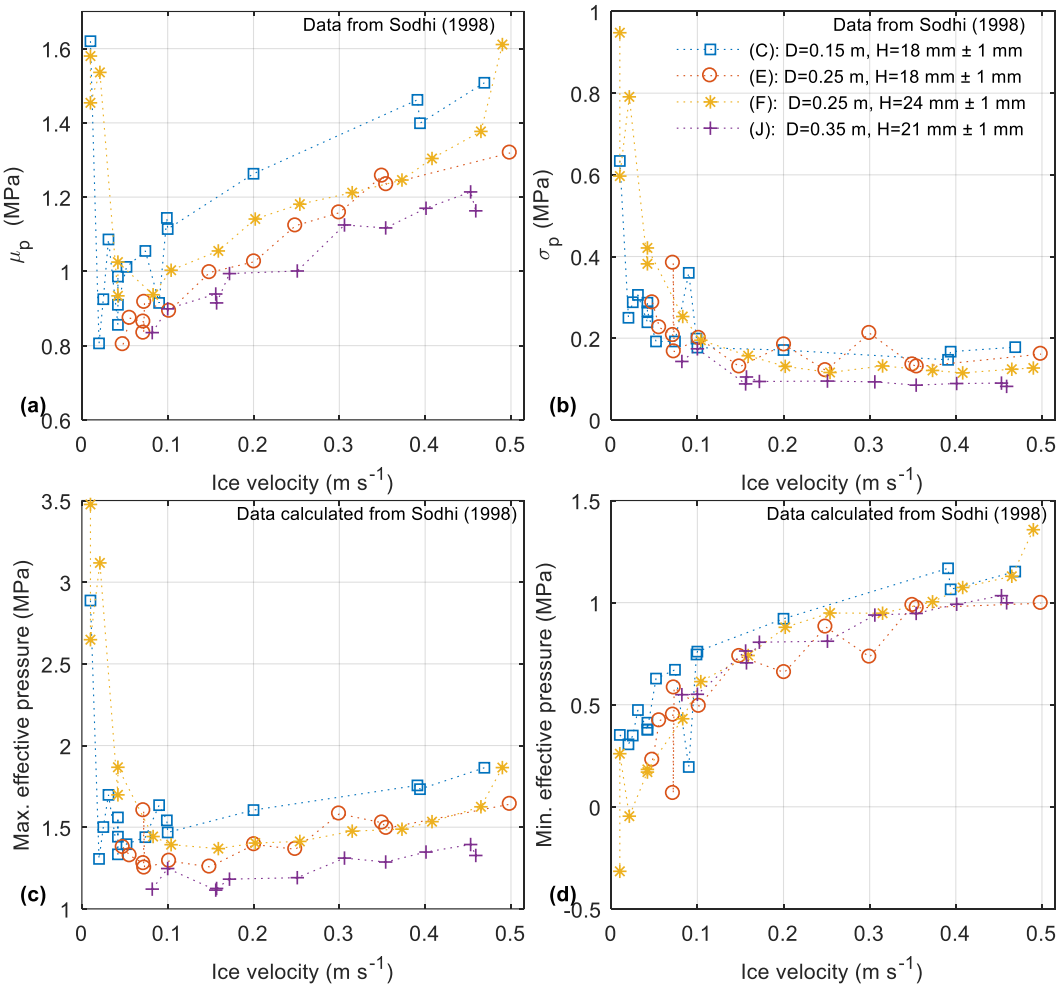

Figure 4.1. Ice velocity vs. the (a) mean, (b) standard deviation, (c) maximum and (d) minimum of effective pressure from the data group of (C), (E), (F) and (J) in Table 4.1.

4.3 Model description

4.3.1 Ice failure zone

The governing equations in the model proposed here are mainly adopted from Ji and Oterkus (2018). There are some improvements between the previous work and the current one. The previous ice failure length, $L = 2H(v_0/v)(K_0/K)$, in the single ice strip model with different structural rigidities and ice velocities were justified in Ji and Oterkus (2018). The constant of 2, as Sodhi used, was in the range of 1-3 in the experiment. Therefore, c is assumed to follow a normal relationship in the range of 1-3. As shown in Figure 4.2, the ice sheet is modelled as multiple strips moving towards a mass-spring-damper idealized structure. Each ice strip is assumed to be independent

of each other and fails at a normally distributed random length of L_i, as specified in Eq. (4.1)

$$L_i = cH(v_0 / v)(K_0 / K) \tag{4.1}$$

where L_i is the ice failure length of each strip, c is a variable distributed normally in the form of $c \sim N(\mu, \sigma_s^2)$ with mean μ and variance σ_s^2, v_0 is the reference velocity, v is the ice velocity, K_0 is the reference stiffness and K is the structural stiffness.

As shown in Figure 4.1 (b), the decreasing standard deviation is related with the decreasing size of ice failure zone. Therefore, it is presumed that ice sheet fails at smaller ice failure zones with higher ice speed with the dimension of $L_i \times W_i \times H$, as illustrated in Figure 4.2, where the width of an ice failure zone W_i is equal to the structural width D over the number of ice strips, i.e. $W_i = D/N_{strip}$. Besides a decreasing ice failure length with increasing ice speed relationship, the width W_i is also assumed to be inversely proportional to the ice velocity$v$. In other words, the number of ice strips N_{strip} is proportional to ice velocity v, as specified in Eq. (4.2), which means that there are more ice strip failures across the interaction surface as the ice speed increases,

$$N_{strip} = (20v + 1)N_{\text{seg}} \tag{4.2}$$

where N_{seg} is the corresponding number of segments in Sodhi's experiment and each segment has a width of 50 mm, i.e. N_{seg}= 1, 3, 5, 7 at D= 50, 150, 250 ,350 mm, respectively. The constant 20 is calibrated based on the comparison between numerical and experimental results and N_{strip} should be round up to an integer during calculation in the case of a decimal value.

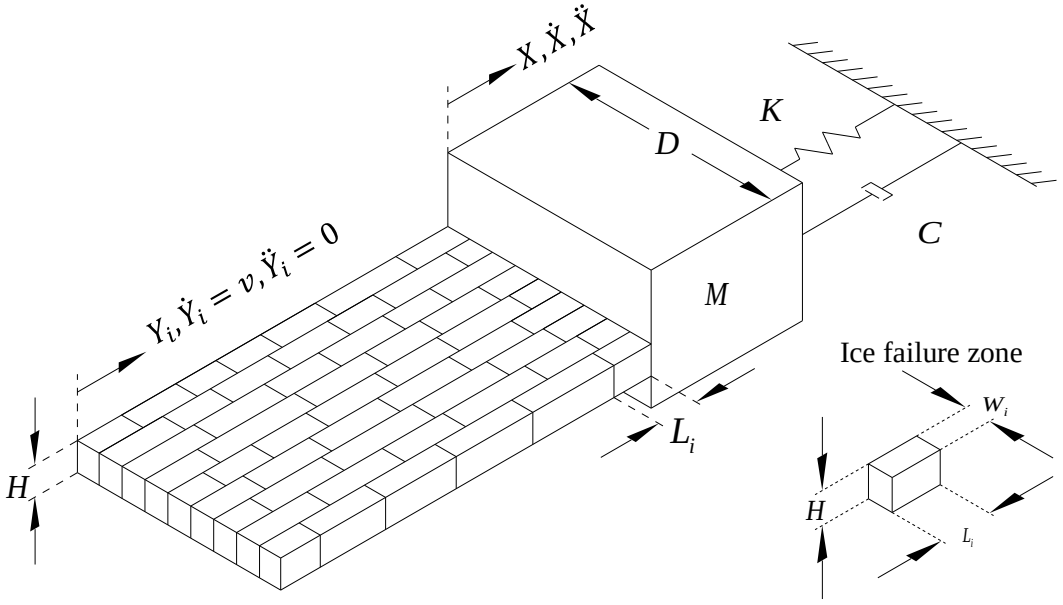

Figure 4.2. Schematic sketch of non-simultaneous dynamic ice-structure model.

4.3.2 Governing equation

In this study, compared with the model in Ji and Oterkus (2018), the ice sheet is extended to multiple strips for non-simultaneous failure characteristics in Eq. (4.3) and (4.4). Each ice failure zone applies a local ice force to the structure that is controlled by the product of area and stress and the variable q_i from Van der Pol oscillator equation adjusted by a magnification factor A. By adding up each local ice force, the total ice force will result in the structure to vibrate in a single degree-of-freedom first-mode motion. The Van der Pol equation is an oscillator with non-linear damping to describe the saw-tooth ice force fluctuation characteristic. There are internal and external effects regarding the oscillator in Eq. (4.4). Internal effect is an assumption that ice has its own original failure characteristic length which corresponds to the oscillator without relative velocity related forcing term on the right-hand side of the oscillator equation. By considering internal effect only, the ice failure frequency can be calculated using the relationship $f_i = v/L_i$. External effect corresponds to structural effects including structural displacement and structural velocity, i.e. relative displacement and relative velocity between ice and structure. Relative velocity takes effect in the forcing term of the Van der Pol oscillator and ice strain rate-stress function in Eq. (4.6). Relative displacement reflects to compressive stress resulting in ice deformation and when the deformation exceeds the ice failure length L_i, ice failure

occurs. Therefore, each ice failure zone will fail under both internal and external effects.

$$M\ddot{X} + C\dot{X} + KX = \sum_{i=1}^{N_{strip}} AHW_i\sigma(q_i + a) \tag{4.3}$$

$$\ddot{q}_i + \varepsilon\omega_i(q_i^{\,2} - 1)\dot{q}_i + \omega_i^{\,2}q_i = \frac{B\omega_i}{H}(\dot{Y}_i - \dot{X}) \tag{4.4}$$

In Eq. (4.3) and Eq. (4.4), M is the mass of the structure, X is the displacement of the structure, the "dot" symbol represents the derivative with respect to time T, C is the damping coefficient, A is the magnification factor for oscillator variable adjusted from experimental data, H is the ice thickness, σ is the variable ice stress satisfying Eq. (4.6), N_{strip} is the number of ice strips, q_i is the dimensionless fluctuation variable of each ice strip, a and ε are scalar parameters that control the lower bound of ice force value and saw-tooth ice force profile, respectively. Since Figure 4.1 (d) shows that the minimum effective pressure increases with increasing velocity, the lower bound a is assumed to increase linearly with ice velocity, as specified in Eq. (4.5), where the coefficients are calibrated based on the comparison between numerical and experimental results for Test. 582, 576, 764 and 763.

$$a(v) = 7v + 4/3 \tag{4.5}$$

$\omega_i = 2\pi f_i$ is the angular frequency of each ice strip force at each particular ice failure length, $f_i = v/L_i$ is the frequency of each ice strip force, B is a coefficient depending on ice properties and Y_i is the displacement of each ice strip. In conjunction with the ice stress power functions (Huang and Liu, 2009),

$$\sigma = \begin{cases} (\sigma_{\max} - \sigma_d)(v_r / v_t)^{\alpha} + \sigma_d, & v_r / v_t \le 1 \\ (\sigma_{\max} - \sigma_b)(v_r / v_t)^{\beta} + \sigma_b, & v_r / v_t > 1 \end{cases} \tag{4.6}$$

where σ_{max} is the maximum stress at ductile-brittle range, σ_d and σ_b are the minimum stress at ductile and maximum stress at brittle range, respectively, $\alpha$and β are positive and negative indices to control the envelope profile, respectively, and v_t is the transition ice velocity approximately in the middle of transition range. Further justification of the parameters are provided in detail in the next section.

4.3.3 Parameter values

The parameters in Eq. (4.1-4.4) and Eq. (4.6) are determined and calibrated by the experimental results summarized in Sodhi (1998). The mass of the structure $M =$

600 kg and damping ratio $\xi = 0.1$ are found in the earlier experimental configuration in Sodhi (1991b). Ice velocity, ice thickness, structural stiffness and structural width are directly used from the Table 4.1. Values of A, a, ε and B are used directly from Ji and Oterkus (2018). K_0, α and β are adjusted by the preliminary simulation results from Test. 582 and Test. 576. Stress variations range is approximately from 1.6 MPa to 4.5 MPa and there is a clear boundary between higher and lower stress value at the velocity of 0.03 m s^{-1}. Therefore, v_t =0.03 m s^{-1}, $\sigma_{\min}$=1600 kPa and $\sigma_{\max}$=4500 kPa are used for the minimum and maximum stress, respectively. As suggested in Sodhi (1998), v_0 =0.03 m s^{-1} and c varies between 1 to 3. Therefore, the mean value is set to $\mu = 2$ and standard deviation is $\sigma_s = 0.3$. A summary of parameter values is listed below:

$M = 600$ kg, $\xi = 0.1$, $K = 35000$ kN m^{-1}, $A = 0.19$, $\varepsilon = 4.6$, B = 0.1;
$\sigma_d = 2000$ kPa, $\sigma_b = 1600$ kPa, $\sigma_{\max} = 4500$ kPa, $\alpha = 0.5$, $\beta = -0.7$, $v_t = 0.03$ m s^{-1};
$v_0 = 0.03$ m s^{-1}, $K_0 = 10000$ kN m^{-1}, $\mu = 2$, $\sigma_s = 0.3$.

4.4 Results and discussion

Based on the experimental results summarized in Table 4.1, four different tests, Test. 582, 576, 764 and 763, are considered. To differentiate the number of numerical simulation and the experimental test, the reproduced numerical results from the corresponding tests are named after STest. and with the corresponding test number, i.e. numerical simulation STest. 582 for experimental Test. 582. Results obtained from the current numerical model are shown in Figures 4.3-4.6. Each figure contains time history plot of total ice force, ice force on each segment and structural displacement. Comparison between numerical results and experiments shows quantitive agreement with the envelope profile of all forces and structural displacements. The mean value F_μ and standard deviation F_σ of ice force are listed in Table 4.2, in which the force is calculated by the product of interaction area and effective pressure. The difference between the results from the model and experiment for F_μ and F_σ, i.e. ΔF_μ and ΔF_σ, are also listed to show the error rate of results.

Table 4.2. Results from experimental tests and numerical simulations.

No.	Test.		STest.		ΔF_μ	ΔF_σ
	F_μ (kN)	F_σ (kN)	F_μ (kN)	F_σ (kN)		
582	7.856	2.354	7.77	2.675	-1.10%	13.62%
576	11.721	1.093	11.712	0.904	-0.08%	-17.31%
764	8.952	3.008	8.875	2.914	-0.86%	-3.11%
763	12.982	0.970	12.438	0.822	-4.19%	-15.28%

Although force records in Figure 4.3 and 4.4 are showing non-simultaneous characteristic in general, there are still different levels of simultaneousness if only one cycle of failure is considered. Force records in STest. 582 show that there is occurrence of a sudden peak force on all segments simultaneously, resulting in large amplitude of force upon the structure, whereas peak force occurs randomly in STest. 764 upon different segments of the structure.

The pattern of smaller variations and higher mean value of ice force with increasing ice velocity coincides with the test results, as shown in Figure 4.3 and 4.5 as well as Figure 4.4 and 4.6. However, as Sodhi mentioned, variations of ice force should decrease when structural width becomes larger, as in STest. 576 and STest.763 shown in Figure 4.5 and 4.6, respectively. On the contrary, both numerical and test results from Test. 764 and STest.764 have higher standard deviation than that from Test. 582 and STest. 582. The reason is that figures in Sodhi (1998) are just plotted in one second. Moreover, the starting and ending time in those figures are not picked at the same time period which makes the statistics less accurate. Because of the randomness in the numerical model, the occurrence and quantity of those four typical ice forces would appear randomly at both STest. 582 and STest. 764. This means that the randomness would exist in the real experiment.

Moreover, it can be noticed that there is more non-simultaneous failure in STest. 764 (Figure 4.4) than that in STest. 582 (Figure 4.3) and in STest. 763 (Figure 4.6) than STest. 576 (Figure 4.5), respectively. Due to increasing ice speed and structural width, the size of ice failure zone becomes smaller, i.e. the number of ice failure zone increases. Hence, the possibility of non-simultaneous failure increases and variation of ice force decreases. Similarly, ice-velocity effect on the size of ice failure zones can also be the reason of different ice failure modes at different speeds. As the size of ice

failure zone decreases with increasing ice speed, ice will fail from larger size to smaller size, which corresponds to the ductile bending mode to brittle crushing mode, respectively. Technically, a cycle of simultaneous ice failure will reduce back to zero value entirely after the unloading phase. There are two reasons of this lower bound of ice force variations. One is attributed to the non-simultaneous characteristic where there are some ice zones remaining in contact with the structure before failure occurs. The other is purely physical contact with the structure leading to high level of ice force.

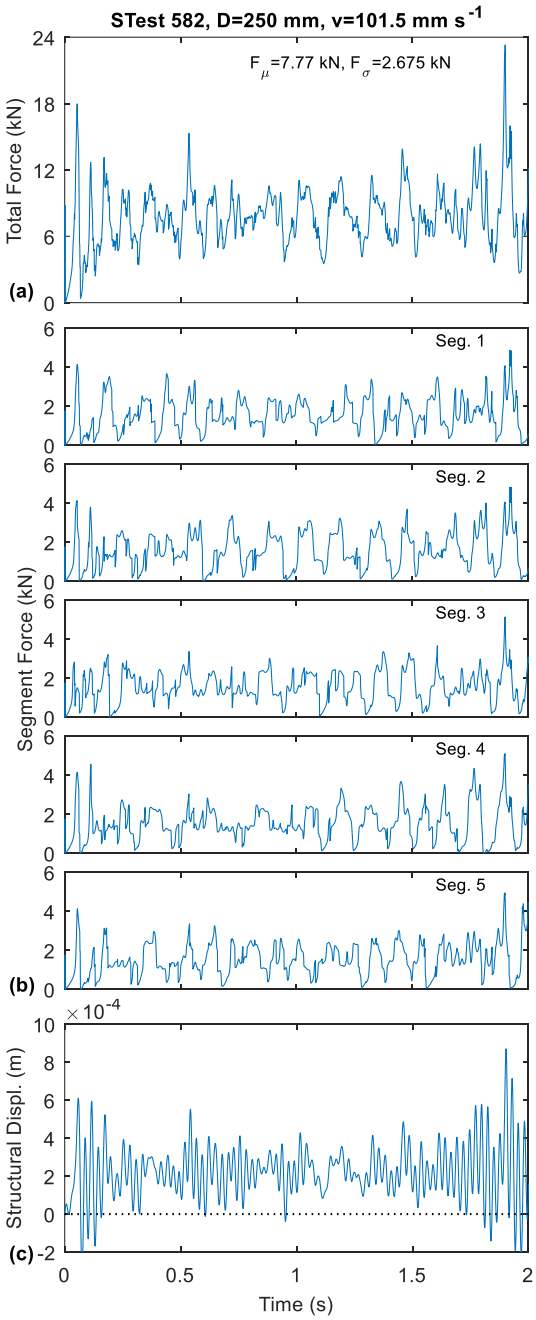

Figure 4.3. Time history of (a) total ice force; (b) ice force on each segment; (c) structural displacement with 5 segments at $\boldsymbol{D}$= 250 mm, $\boldsymbol{v}$= 101.5 .m s^{-1}.

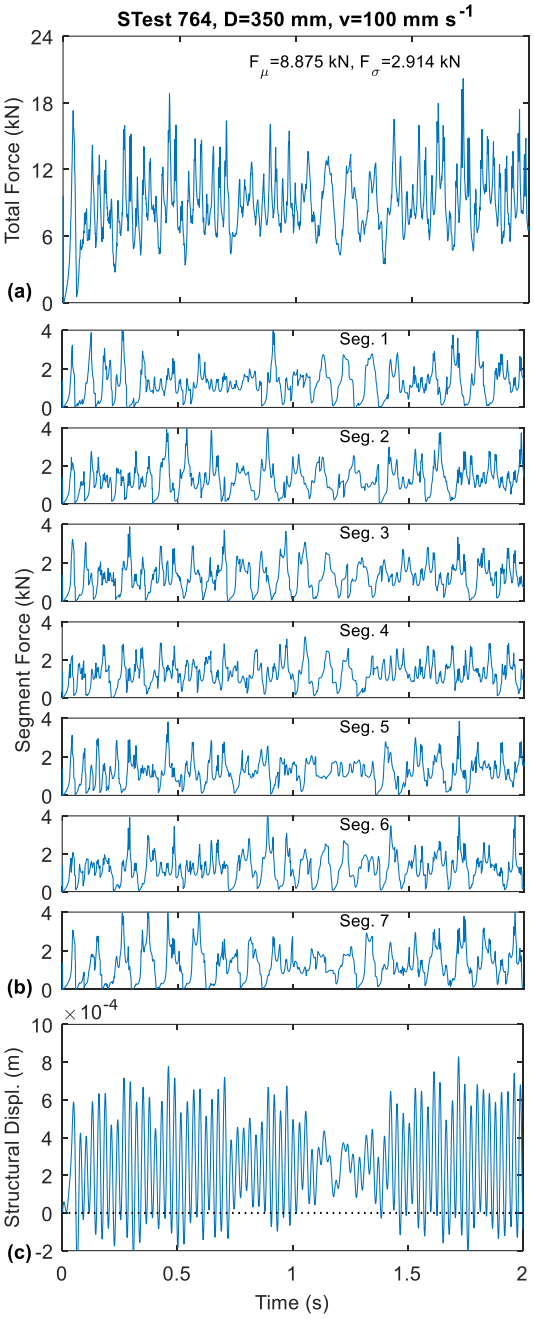

Figure 4.4. Time history of (a) total ice force; (b) ice force on each segment; (c) structural displacement with 7 segments at $\boldsymbol{D}$= 350 mm, $\boldsymbol{v}$= 100 mm s^{-1}.

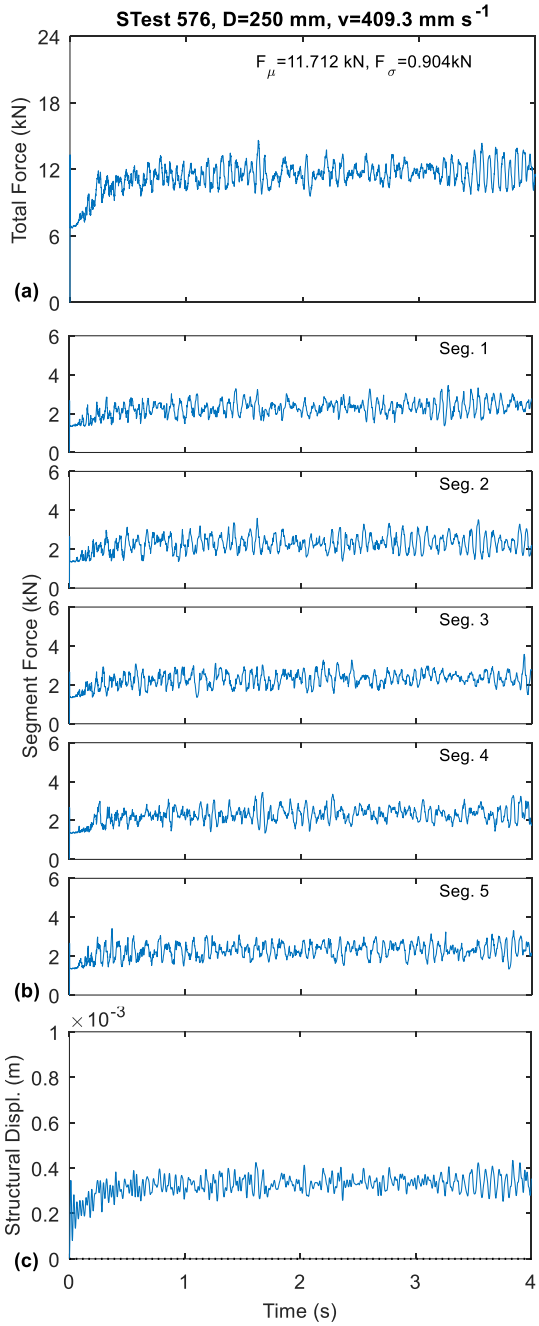

Figure 4.5. Time history of (a) total ice force; (b) ice force on each segment; (c) structural displacement with 5 segments at $\boldsymbol{D}$= 250 mm, $\boldsymbol{v}$= 409.3 mm s^{-1}.

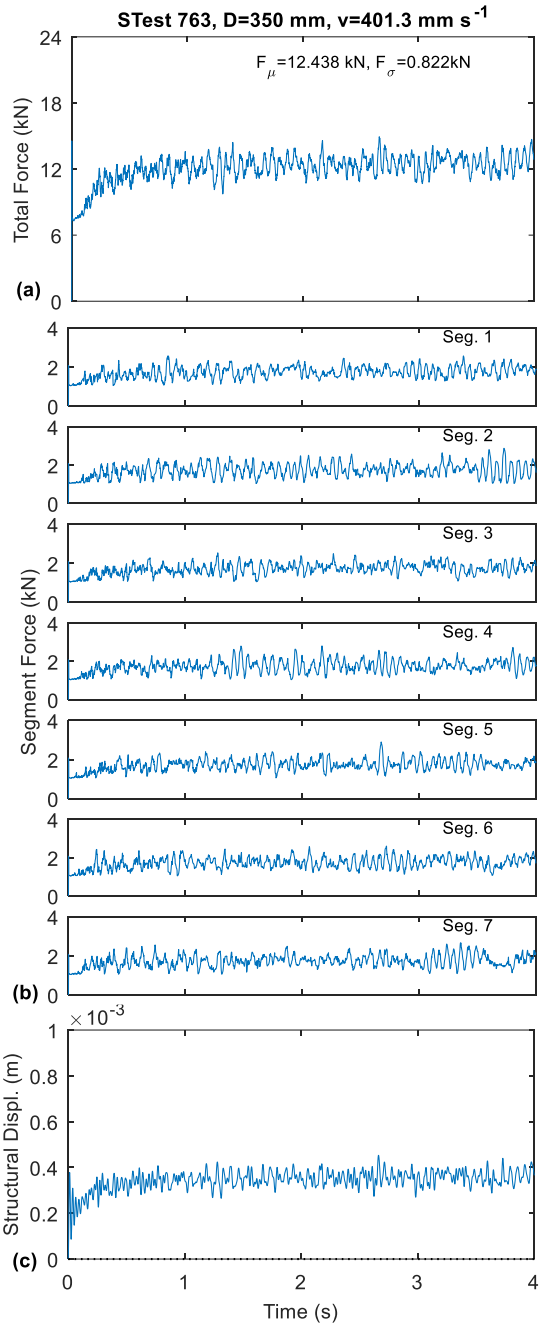

Figure 4.6. Time history of (a) total ice force; (b) ice force on each segment; (c) structural displacement with 7 segments at $\boldsymbol{D}$= 350 mm, $\boldsymbol{v}$= 401.3 mm s^{-1}.

4.5 Demonstration cases

To test the calibrated model's capability at different D, H and v, it is used to simulate 134 different tests from Group (A) to (K) in Table 4.1. Same configurations as those in the previous four simulations are used by only changing the D, H and v. Figure 4.7 (a-k) show a series of comparisons of μ_p and σ_p between the model (plotted in red) and experiment (plotted in blue) as the ice velocity increases. The model captures the general trend of μ_p and σ_p as v increases, especially at some fluctuation points. Meanwhile, there are some abnormal experimental results that require a double-check, such as the peak points in Figure 4.7 g(1) and h(2). The μ_p and σ_p have better accuracy as the ice velocity increases, as shown in Figure 4.8. The difference between the results from model and experiment for μ_p and σ_p, i.e. $\Delta\mu_p$ and $\Delta\sigma_p$, are plotted against v with the mean of -6.05% and 11.42% difference, respectively.

Figure 4.9 shows the histogram of the $\Delta\mu_p$ and $\Delta\sigma_p$ with an interval of 10% between each bar. The number on the top of each bar shows the corresponding percentage weighted among all data. The model can predict well on the mean value that 76.8% of data yield a value within 20% of difference between the model and experiment. In terms of σ_p, 71% of data yield a value within 50% of difference and 30.7% of data yields a value within the 20% of difference. The less accuracy at lower velocity range can be the reason of corresponding ductile ice failure property. The failure mechanism in the numerical model is supposed to simulate the crushing brittle ice failure behaviour, in which ice fails at certain amount of length.

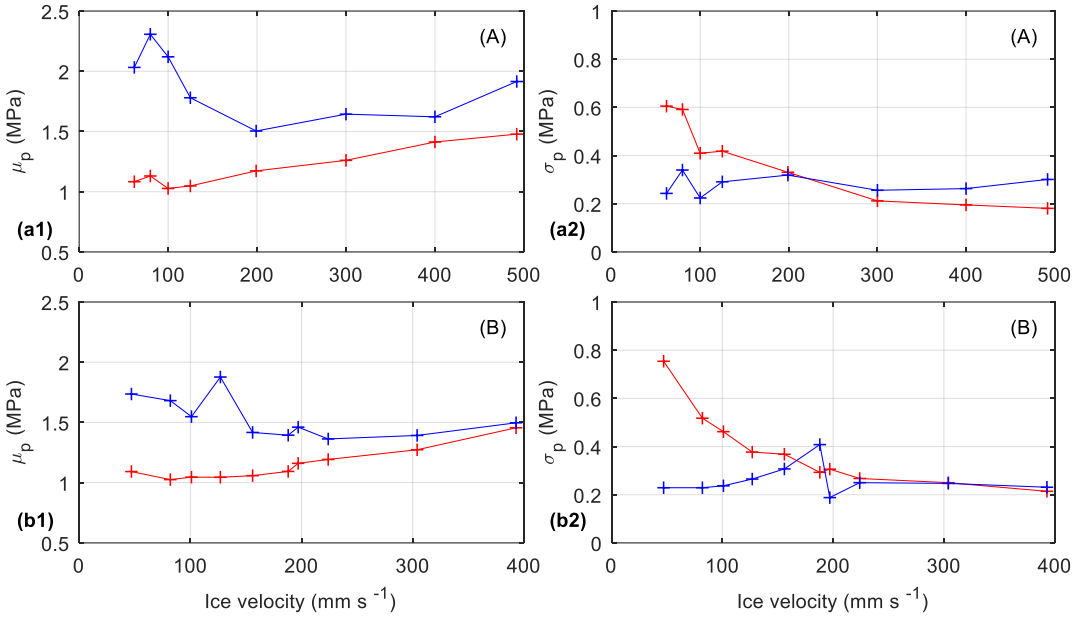

Figure 4.7. (a-b) *D*=50 mm.

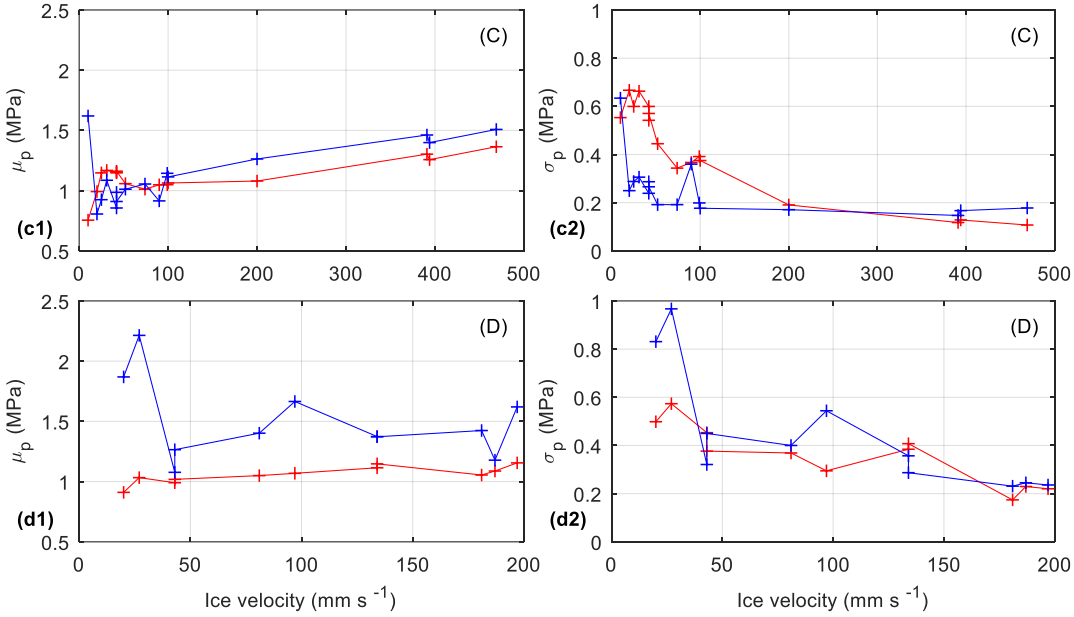

Figure 4.7. (c-d) *D* =150 mm.

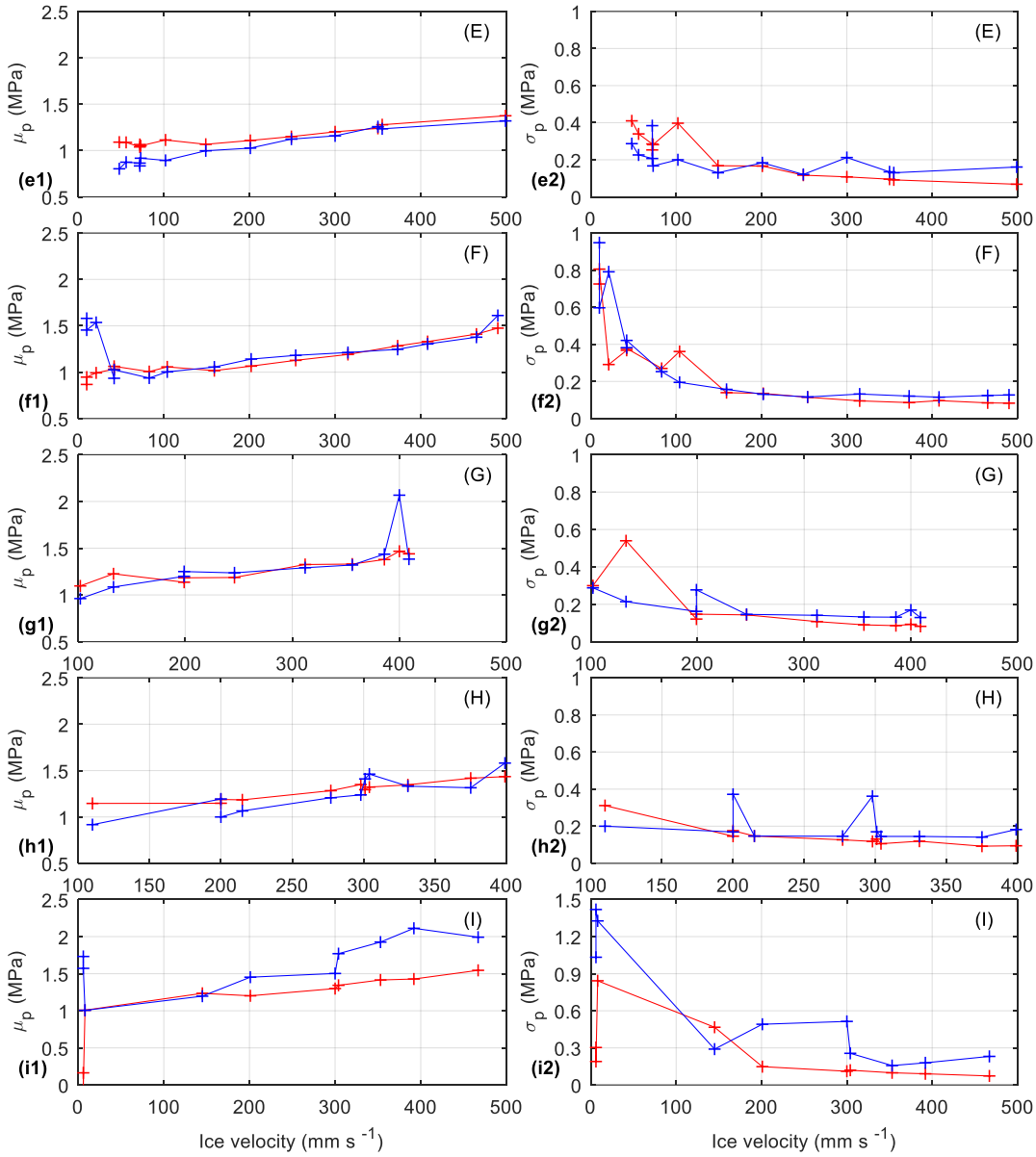

Figure 4.7. (e-i) *D* =250 mm.

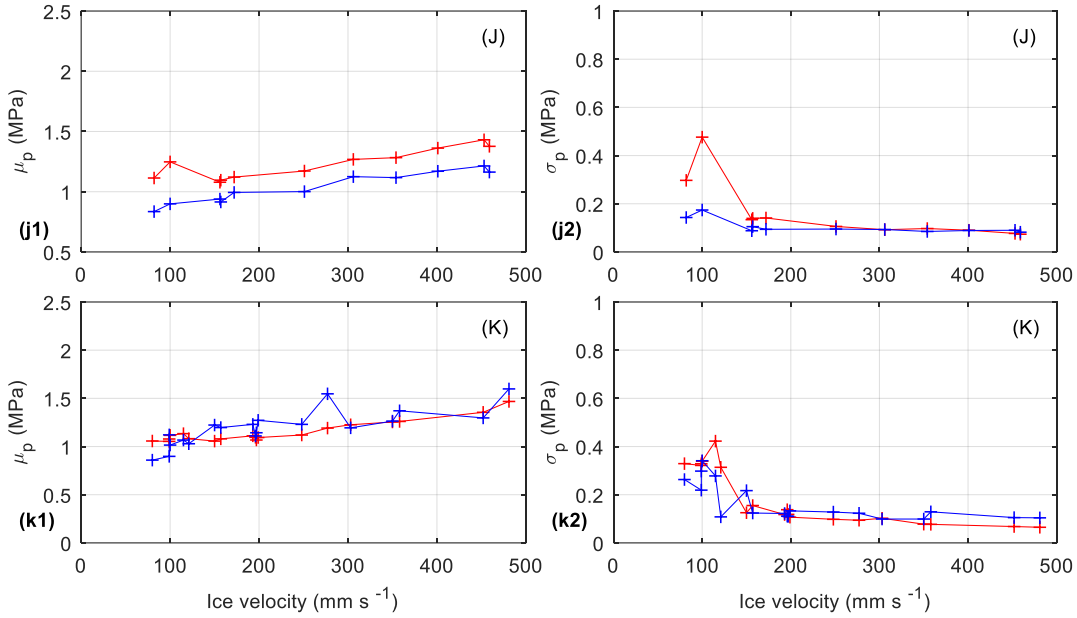

Figure 4.7. Ice velocity vs. the mean $\boldsymbol{\mu_p}$ and standard deviation $\boldsymbol{\sigma_p}$ of the effective pressure across the interaction surface from numerical simulations (red line) and experimental results (blue line), at (a-b) *D*=50 mm, (c-d) *D* =150 mm, (e-i) *D* =250 mm, (j-k) *D* =350 mm with the corresponding data group of (A) to (K) from Table 4.1.

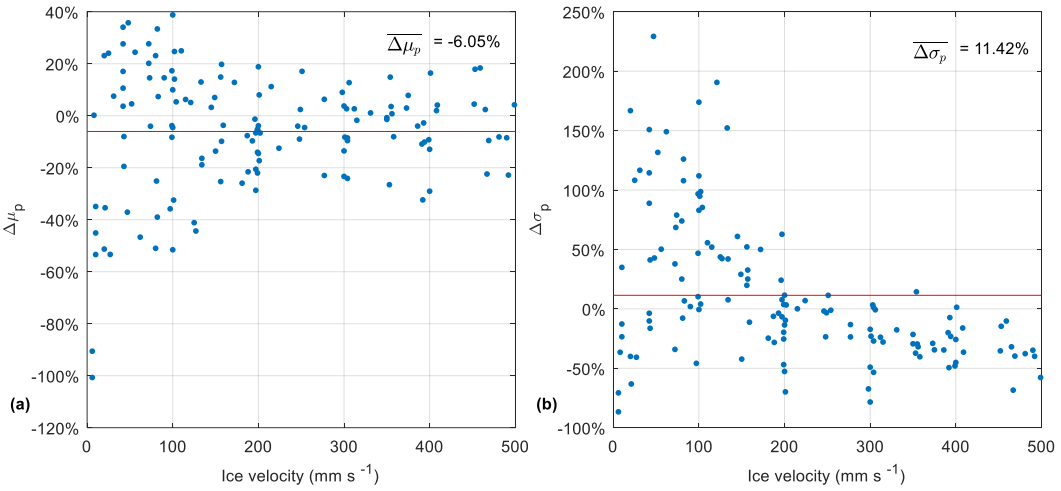

Figure 4.8. Ice velocity vs. (a) mean and (b) standard deviation of the effective pressure difference (in percentage) between numerical simulations and experimental results.

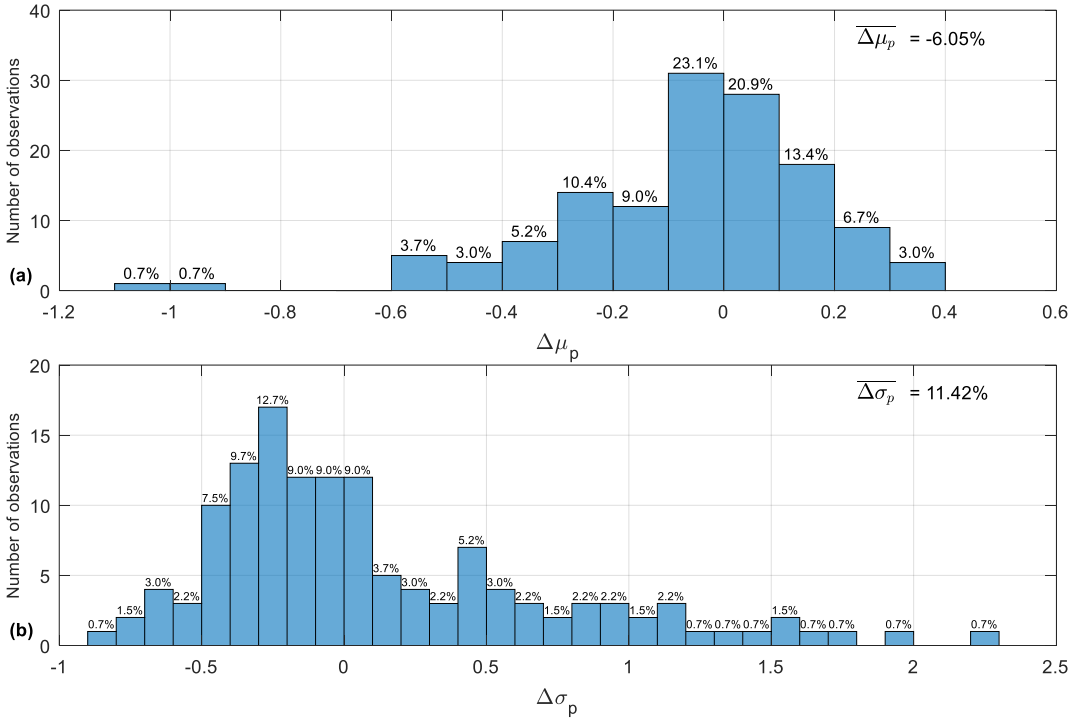

Figure 4.9. Ice velocity vs. (a) mean and (b) standard deviation of the effective pressure difference (in percentage) between numerical simulations and experimental results.

4.6 Summary

To simulate non-simultaneous ice failure effects on ice-structure interaction, an extended model based on the previous work of Ji and Oterkus (2018) was developed. An assumption was made that the size of ice failure zone will decrease when ice velocity increases. Therefore, the ice failure length and width of each individual zone decreases, which increase the possibility of non-simultaneous effect on ice failure. Numerical results agree well with experiment data in Sodhi (1998) and indicates that variations of ice force decrease with increasing ice velocity and increasing structural width, respectively. There is simultaneous failure occurrence on all segments at lower ice velocity, indicating large size of ice failure zone at ductile bending failure mode. At higher ice velocity, there is more random peak forces taking place on different segments, indicating more non-simultaneous ice failures at smaller brittle crushing zones. The simulation results from a series of 134 blind tests demonstrate the model's capability of predicting at different ice velocities, structural widths and ice thicknesses. In addition, analysis of the ice indentation experiments shows that the mean and

minimum effective pressure have an approximately linear relationship with ice velocity which testified the assumption on variations of ice failure zone in the model.

CHAPTER

5. CONCLUSIONS

5.1 Achievements against the objectives

As described in the Chapter 1, the goal of this research was to produce unconventional and more effective numerical frameworks that can be helpful in ice-structure engineering in the shipping and offshore industry. The list here below summarises the main achievements of this work, which are in line with the research objectives:

- A novel single degree-of-freedom dynamic ice-structure interaction model was developed on the basis of a physical mechanism combination between self-excited vibration and forced vibration. The model was able to capture the three different structural responses and the lock-in phenomenon in IIV.
- An improved ice failure function was integrated into the previous model by considering ice velocity and structural natural frequency effect. The new model was able to accurately reproduce three basic modes of response, i.e. intermittent crushing, frequency lock-in and continuous crushing.
- Discussions and explanations of the physical mechanism of dynamic ice-structure interaction at three distinctive modes of response were presented, especially the mechanics when IIV occurs. This is the first time in the past half century that force vibration and self-excited vibration theories are brought together to explain the ice mechanics.
- A two-dimensional non-simultaneous dynamic ice-structure interaction model was developed based on the previous model to overcome these limitations and produce better correlation with full range of experimental data.

5.2 Novelty and contribution to the field

Ice is so common in life and yet the research of ice started just about 60 years ago and we still struggle with its mechanics as well as its modelling. Kärnä et al. (2013) pointed out that modellers were able to do much better when “fitting” as compare to “predicting”.

A Van der Pol based model had been developed in the above series of work. It is the first time such numerical model is capable of predicting ice force and structural

response under a full range of ice velocities. In addition, ice force frequency lock-in phenomenon was captured at ice-induced vibrations condition. Basic factors, such as ice velocity and structural natural frequency, had been coupled into the model to replace some empirical parameters and improve the accuracy of the results.

On the other hand, physical mechanism of ice-structure interaction and the reason of IIV have been in a debated situation during the past 50 years. Theories and various models were proposed by ice researchers during its heyday in the 80s and 90s. One biggest disagreement is whether IIV is forced or self-excited. To solve this question, a novel explanation of combining those two physical mechanisms was proposed, which varies mainly based on the ice velocity and external structural effect.

5.3 Gaps and future studies

In this study, ice velocity is assumed as far-field velocity of a large ice sheet, in which the velocity stays as a constant value and is not affected by the dynamic response of structure. Since part of the motivation of this research also stems from a potential shipping route through the Arctic Ocean, it is necessary to consider small ice flow interacting with ship hull structure. Therefore, ice velocity is a variable regarding near-filed instant response coming from ship hull. At the same time, floating ice sheet is under the impact of fluid all the time. An ice-fluid-structure coupling model is necessary to fulfil this ice-ship interaction simulation target.

Despite the realistic performance of the novel ice-structure interaction model developed in this work, some empirical parameters were used for its realisation. Instead, more sophisticated functions should be coupled with the presented Van der Pol based frameworks to reproduce and investigate their performance further in a laboratory environment. In addition to the equation in ISO 19906(2010), there should be a number like Strouhal to determine the situation when IIV will occur regardless of the scale. As Ji and Oterkus (2018) mentioned, the characteristic of ice force formation has a strong relationship with frictional force between the ice and the interaction surface as well as within the ice itself. In particular, IIV is analogous to friction-induced vibration in many ways. Therefore, experimentation is required to study this mechanics.

5.4 Research outputs

Journal articles

- **Ji, X**., Karr, D.G. and Oterkus, E., 2018. A non-simultaneous dynamic ice-structure interaction model. *Ocean Engineering*, 165, 278-289, doi.org/10.1016/j.oceaneng.2018.08.032.
- **Ji, X**., Oterkus, E., 2018. Physical mechanism of ice/structure interaction. *Journal of Glaciology*, 64, 197-207. doi.org/10.1017/jog.2018.5.
- **Ji, X**., Oterkus, E., 2016. A dynamic ice-structure interaction model for ice-induced vibrations by using van der pol equation. *Ocean Engineering*, 128, 147-152. doi.org/10.1016/j.oceaneng.2016.10.028.

Conference proceedings/presentations

- **Ji, X**., Karr, D.G. and Oterkus, E, 2018. A dynamic ice-structure interaction model for non-simultaneous ice failure. 28th International Society of Offshore and Polar Engineers (ISOPE). Sapporo, Japan.
- **Ji, X**., Oterkus, E., 2017. A new van der Pol equation based ice-structure interaction model for ice-induced vibrations. 6th International Conference of Marine Structures (MARSTRUCT). Lisbon, Portugal. 107-111.
- **Ji, X**., Oterkus, E., 2016. A novel dynamic ice-structure interaction model for ice-induced vibrations. 16th Techno-Ocean Conference, Kobe, Japan. New York: IEEE, 70-73.
- Oterkus, E., Vazic, B., **Ji, X**. and Oterkus, S., 2017, Peridynamic Modelling of Ice Fracture, Ice Fracture and Cracks Workshop (SIPW04), Isaac Newton Institute for Mathematical Sciences, Cambridge, UK.
- Vazic, B., **Ji, X**., Oterkus, E. and Oterkus, S., 2017, Ice-Structure Interactions by using Peridynamics, ASME 2017 International Mechanical Engineering Congress & Exposition, Tampa, FL, USA.
- Vazic, B., **Ji, X**., Diyaroglu, C., Oterkus, S. and Oterkus, E., 2016, Ice fracture modelling by using Peridynamics, ASME 2016 International Mechanical Engineering Congress & Exposition, Phoenix, USA.

5.5 Final remarks

In a nutshell, this Van der Pol based model is more powerful than the others in kind by far because of its accurate results, wide applicability and novel physical mechanism

behind. Thus, the numerical models produced as part of this research can be helpful in ice failure analysis and in the design of ice-resistant structures.

REFERENCES

Ashby, M., Palmer, A., Thouless, M., Goodman, D., Howard, M., Hallam, S., Murrell, S., Jones, N., Sanderson, T., Ponter, A., 1986. Nonsimultaneous failure and ice loads on arctic structures, Offshore Technology Conference. Offshore Technology Conference.

Bhat, S., 1990. Modeling of size effect in ice mechanics using fractal concepts. Journal of Offshore Mechanics and Arctic Engineering 112 (4), 370-376.

Blenkarn, K., 1970. Measurement and analysis of ice forces on Cook Inlet structures, Offshore Technology Conference. Offshore Technology Conference.

Coburn, J.L., Jr, R.P.J., Baird, A.V., Jizu, X., Shuqi, D., Tongkiu, L., Fucheng, L., 1984. Bohai Sea Ice Design Criteria.

Den Hartog, J., 1947. Mechanical Vibrations, 3rd ed. McGraw-Hill, New York.

Ding, W., 2012. Self-excited vibration : theory, paradigms and research methods. Springer, New York; London.

Hendrikse, H., Kuiper, G., Metrikine, A., 2011. Ice induced vibrations of flexible offshore structures: the effect of load randomness, high ice velocities and higher structural modes, 21st International Conference on Port and Ocean Engineering Under Arctic Conditions, p. 031.

Huang, G., Liu, P., 2009. A dynamic model for ice-induced vibration of structures. Journal of Offshore Mechanics and Arctic Engineering 131 (1), 011501.

Huang, Y., Shi, Q., Song, A., 2007. Model test study of the interaction between ice and a compliant vertical narrow structure. Cold regions science and technology 49 (2), 151-160.

Ji, X., Dale, K., Oterkus, E., 2018. A non-simultaneous dynamic ice-structure interaction model. Ocean Engineering 166, 278-289.

Ji, X., Oterkus, E., 2016. A dynamic ice-structure interaction model for ice-induced vibrations by using van der pol equation. Ocean Engineering 128, 147-152.

Ji, X., Oterkus, E., 2018. Physical mechanism of ice/structure interaction. Journal of Glaciology 64 (244), 197-207.

Johansson, P., 1981. Ice-induced vibration of fixed offshore structures, part 1: review of dynamic response analyses, Marine Structures and Ships in Ice.

Johnston, M., Croasdale, K.R., Jordaan, I.J., 1998. Localized pressures during ice–structure interaction: relevance to design criteria. Cold regions science and technology 27 (2), 105-117.

Kärnä, T., 2001. Simplified modelling of ice-induced vibrations of offshore structures, 16th International Symposium on Okhotsk Sea & Sea Ice, Mombetsu, Japan, pp. 114-122.

Kärnä, T., 2007. Research Problems Related to Time-Varying Ice Actions, Proceedings of the International Conference on Port and Ocean Engineering Under Arctic Conditions.

Kärnä, T., Andresen, H., Gurtner, A., Metrikine, A., Sodhi, D., Loo, M., Kuiper, G., Gibson, R., Fenz, D., Muggeridge, K., 2013. Ice-Induced Vibrations of Offshore Structures–Looking Beyond ISO 19906, 22nd International Conference on Port and Ocean Engineering Under Arctic Conditions (POAC), Espoo, Finland, pp. 1673-1684.

Kärnä, T., Muhonen, A., Sippola, M., 1993. Rate effects in brittle ice crushing, Conf. Port Ocean Eng. under Arctic Conditions. (POAC´93), Hamburg, pp. 59-71.
Kärnä, T., Trunen, R., 1990. A straightforward technique for analyzing structural response to dynamic ice action, Proceedings of the Ninth International Conference on Offshore Mechanics and Arctic Engineering (OMAE), pp. 135-142.
Karr, D.G., Troesch, A.W., Wingate, W.C., 1993. Nonlinear dynamic response of a simple ice-structure interaction model. Journal of Offshore Mechanics and Arctic Engineering 115 (4), 246-252.
Kry, P., 1978. A Statistical Prediction of Effective Ice Crushing Stresses on Wide Structure, Proc. of IAHR Ice Symposium.
Kry, P., 1980. Third Canadian geotechnical colloquium: Ice forces on wide structures. Canadian Geotechnical Journal 17 (1), 97-113.
Kry, P., 1981. Scale effects in continuous crushing of ice, Proceedings of the Fifth International Association Hydraulic Research Symposium on Ice Problems. Laval University, Quebec, Canada, pp. 27-31.
Määttanen, M., 1975. Experiences of ice forces against a steel lighthouse mounted on the seabed, and proposed constructional refinements, Proc. of the Third Int. Conf. on Port and Ocean Engineering under Arctic Conditions POAC, Fairbanks.
Määttänen, M., 1981. Laboratory tests for dynamic ice-structure interaction. Engineering Structures 3 (2), 111-116.
Määttänen, M., 1983. Dynamic ice-structure interaction during continuous crushing. DTIC Document.
Määttänen, M., 2015. Ice induced frequency lock-in vibrations - Converging towards consensus, Proceedings of the International Conference on Port and Ocean Engineering under Arctic Conditions, POAC.
Matlock, H., Dawkins, W.P., Panak, J.J., 1971. Analytical model for ice-structure interaction. Journal of the Engineering Mechanics Division 97 (4), 1083-1092.
Michel, B., Toussaint, N., 1978. Mechanisms and theory of indentation of ice plates. Journal of Glaciology 19, 285-300.
Neill, C.R., 1976. Dynamic ice forces on piers and piles. An assessment of design guidelines in the light of recent research. Canadian Journal of Civil Engineering 3 (2), 305-341.
Palmer, A., Goodman, D., Ashby, M., Evans, A., Hutchinson, J., Ponter, A., 1983. Fracture and its role in determining ice forces on offshore structures. Annals of Glaciology 4, 216-221.
Palmer, A., Qianjin, Y., Fengwei, G., 2010. Ice-induced vibrations and scaling. Cold regions science and technology 60 (3), 189-192.
Peyton, H.R., 1966. Sea ice forces, Ice pressures against structures. National research council, Quebec, Canada, pp. 117-123.
Rao, S.S., 2004. Mechanical vibrations, 4th ed. Upper Saddle River: Pearson Education, India.
Schmitz, T.L., Smith, K.S., 2011. Mechanical vibrations: modeling and measurement. Springer Science & Business Media, New York.
Sodhi, D.S., 1988. Ice-induced vibrations of structures, Proceedings of the Ninth International Association of Hydraulic Engineering and Research Symposium on Ice, Sapporo, Japan, pp. 625-657.

Sodhi, D.S., 1991a. Energy exchanges during indentation tests in fresh-water ice. Annals of Glaciology 15, 247-253.
Sodhi, D.S., 1991b. Ice-structure interaction during indentation tests, in: Jones S., T.J., McKenna R.F., Jordaan I.J. (Ed.), Ice-Structure Interaction. Springer, Berlin, Heidelberg, pp. 619-640.
Sodhi, D.S., 1994. A theoretical model for ice-structure interaction, 12th International symposium on ice, IAHR 94. Villco Trykkeri AS, Trondheim, Norway, pp. 807-815.
Sodhi, D.S., 1995. An ice-structure interaction model. Studies in Applied Mechanics 42, 57-75.
Sodhi, D.S., 1998. Nonsimultaneous crushing during edge indentation of freshwater ice sheets. Cold regions science and technology 27 (3), 179-195.
Sodhi, D.S., 2001. Crushing failure during ice–structure interaction. Engineering Fracture Mechanics 68 (17), 1889-1921.
Sodhi, D.S., Haehnel, R.B., 2003. Crushing ice forces on structures. Journal of Cold Regions Engineering 17 (4), 153-170.
Sodhi, D.S., Morris, C.E., 1986. Characteristic frequency of force variations in continuous crushing of sheet ice against rigid cylindrical structures. Cold regions science and technology 12 (1), 1-12.
Sodhi, D.S., Nakazawa, N., 1990. Frequency of intermittent ice crushing during indentation tests, Proc. 10th IAHR Symposium on Ice, Espoo, Finland, pp. 277-290.
Sukhorukov, S., 2013. Ice-Ice and Ice-Steel Friction in Field and in Laboratory, Department of Civil and Transport Engineering. Norwegian University of Science and Technology, Trondheim, Norway.
Timco, G., Johnston, M., 2004. Ice loads on the caisson structures in the Canadian Beaufort Sea. Cold regions science and technology 38 (2), 185-209.
Timoshenko, S., Young, D., 1937. Vibration Problems in Engineering, (1937). D van Nostrand Company, Inc., New-York.
Tong, J., Song, A., Shi, Q., 2001. An experimental study of ice-induced vibration and dynamic characteristics of ice loads. Ocean Eng 19, 34-39.
Tsuchiya, M., Kanie, S., Ikejiri, K., Ikejiri, A., Saeki, H., 1985. An experimental study on ice-structure interaction, Offshore Technology Conference.
Wang, L., Xu, J., 1991. Description of dynamic ice-structure interaction and the ice force oscillator model, 11 th International Conference on Port and Ocean Engineering under Arctic Conditions, St. John's, Canada, pp. 141-154.
Withalm, M., Hoffmann, N., 2010. Simulation of full-scale ice–structure-interaction by an extended Matlock-model. Cold regions science and technology 60 (2), 130-136.
Yu, B., Karr, D., 2014. An ice-structure interaction model for non-simultaneous ice failure, OTC Arctic Technology Conference. Offshore Technology Conference, p. 24547.
Yue, Q., Guo, F., 2011. Physical Mechanism of Ice-Induced Self-Excited Vibration. Journal of Engineering Mechanics 138 (7), 784-790.
Yue, Q., Guo, F., Kärnä, T., 2009. Dynamic ice forces of slender vertical structures due to ice crushing. Cold regions science and technology 56 (2), 77-83.